Resource

TRANSPARENT PROCESS SOURCE DATA OPEN ACCESS

Life Science Alliance

Mitochondrial phosphoproteomes are functionally specialized across tissues

Fynn M Hansen[1], Laura S Kremer[2], Ozge Karayel[1], Isabell Bludau[1], Nils-Göran Larsson[2], Inge Kühl[3], Matthias Mann[1]

Mitochondria are essential organelles whose dysfunction causes human pathologies that often manifest in a tissue-specific manner. Accordingly, mitochondrial fitness depends on versatile proteomes specialized to meet diverse tissue-specific requirements. Increasing evidence suggests that phosphorylation may play an important role in regulating tissue-specific mitochondrial functions and pathophysiology. Building on recent advances in mass spectrometry (MS)-based proteomics, we here quantitatively profile mitochondrial tissue proteomes along with their matching phosphoproteomes. We isolated mitochondria from mouse heart, skeletal muscle, brown adipose tissue, kidney, liver, brain, and spleen by differential centrifugation followed by separation on Percoll gradients and performed high-resolution MS analysis of the proteomes and phosphoproteomes. This in-depth map substantially quantifies known and predicted mitochondrial proteins and provides a resource of core and tissue-specific mitochondrial proteins (mitophos.de). Predicting kinase substrate associations for different mitochondrial compartments indicates tissue-specific regulation at the phosphoproteome level. Illustrating the functional value of our resource, we reproduce mitochondrial phosphorylation events on dynamin-related protein 1 responsible for its mitochondrial recruitment and fission initiation and describe phosphorylation clusters on MIGA2 linked to mitochondrial fusion.

DOI 10.26508/lsa.202302147 | Received 9 May 2023 | Revised 3 November 2023 | Accepted 7 November 2023 | Published online 20 November 2023

Introduction

Mitochondria are double-membrane–bound organelles with an essential role in homeostasis of eukaryotic cells. They are often referred to as the "powerhouse of the cell" because of their prominent function in bioenergetics. Among many other processes, they are also involved in several biosynthetic processes such as balancing redox systems, the regulation of metabolic by–products like reactive oxygen species (ROS) (Spinelli & Haigis, 2018) and hold a central role in cell death (Bock & Tait, 2020). The function and stability of mitochondria depend on their intrinsic bioenergetics regulation and finely orchestrated interaction with the cellular microenvironment. Energy conversion via the oxidative phosphorylation system plays an essential role in harvesting energy from ingested nutrients. Moreover, the morphology of mitochondria within an eukaryotic cell is actively regulated by fusion and fission events which dynamically modulate their number, size, and localization (Liesa et al, 2009). Regulation of mitochondrial dynamics also affects the interplay of mitochondria with other cellular structures, such as the cytoskeleton for active regulation of their localization (Moore & Holzbaur, 2018), and organelles like the endoplasmic reticulum (ER) and lipid droplets to regulate many physiological processes such as energy metabolism and ion buffering. The mitochondria-associated membrane, which is the contact site of the outer mitochondrial membrane with the ER, comprises a unique set of proteins mediating this interaction and fine-tunes mitochondrial functions with the cellular microenvironment (Nunnari & Suomalainen, 2012; Kwak et al, 2020). Dysregulation of any of these intricate processes can lead to severe mitochondrial dysfunctions and diseases, including neurodegenerative diseases, cardiovascular disorders, myopathies, obesity, and cancers, which can manifest in a cell type- and tissue-specific manner (Suomalainen & Battersby, 2018).

The fitness of mitochondria depends on the production and maintenance of functional and versatile proteomes specialized to carry out a variety of functions within the eukaryotic metabolism and meet diverse cellular and tissue-specific requirements (Kuznetsov et al, 2009). The mitochondrial proteome includes over a 1,000 proteins (see below), but only a small fraction of 13 proteins are encoded on the circular mitochondrial DNA molecule (Anderson et al, 1981). Thus, most of the mitochondrial proteins are encoded by the nuclear genome, synthesized outside of mitochondria and subsequently imported into the organelle, implying that mechanisms controlling mitochondrial protein quality (e.g., correct protein folding and import) are essential for health and integrity of mitochondria (Jadiya & Tomar, 2020). Furthermore, investigations of mitochondrial dynamics and functional plasticity have revealed regulatory roles for posttranslational modifications, including phosphorylation (Niemi & Pagliarini, 2021). Studies have shown that phosphorylation of several

[1]Department of Proteomics and Signal Transduction, Max Planck Institute of Biochemistry, Martinsried, Germany [2]Department of Medical Biochemistry and Biophysics, Karolinska Institutet, Stockholm, Sweden [3]Department of Cell Biology, Institute of Integrative Biology of the Cell, UMR9198, CEA, CNRS, Université Paris-Saclay, Gif-sur-Yvette, France

Correspondence: mmann@biochem.mpg.de

mitochondrial proteins is involved in the regulation of central processes such as metabolic function, for instance, through phosphorylation of the E1-alpha subunit of PDH (Patel et al, 2014), mitophagy (Kolitsida et al, 2019), and fission (Cribbs & Strack, 2007; Taguchi et al, 2007; Ducommun et al, 2015; Toyama et al, 2016; Lewis et al, 2018). Thus, deregulation of protein phosphorylation might be an important underlying feature of mitochondrial physiology and pathophysiology. Currently, there is a significant knowledge gap of the mitochondrial variable proteomic composition and to what extent it is phosphorylated in a tissue-specific manner and how posttranslational regulation influences organelle function. A detailed understanding of the functional specialization of mitochondria at the protein and phosphorylation levels is needed to elucidate the contribution of mitochondria to health and disease.

Large-scale mass spectrometry (MS)-based quantitative proteomics studies from our and other groups have already shed light on the proteomic composition of mitochondria of various mammalian tissues and cell types, mostly highlighting that most of the proteins are shared between mitochondria of different tissues (Mootha et al, 2003; Forner et al, 2006; Pagliarini et al, 2008). The breadth and depth of such studies has been largely driven by technological advances in the field in combination with improvements of mitochondria isolation procedures, such as differential centrifugation (DC), DC in conjunction with ultracentrifugation on, for example, Percoll gradients, magnetic bead-assisted methods (MACS) (Kappler et al, 2016) or MitoTags (Bayraktar et al, 2019). Efforts in defining the mitochondrial proteome lead to databases like MitoCarta2.0 and IMPI (http://impi.mrc-mbu.cam.ac.uk/), both integrated in Mitominer4.0 (Smith & Robinson, 2019). A recent quantitative and high confidence proteome of human mitochondria identified 1,134 different proteins that vary over six orders in magnitude in abundance (Morgenstern et al, 2021). Similarly, efforts have been undertaken to map the mitochondrial phosphoproteome and identify dozens to hundreds of phosphorylation sites on mitochondrial proteins (listed in Table S1 [Schulenberg et al, 2003; Hopper et al, 2006; Lee et al, 2007; Feng et al, 2008; Lewandrowski et al, 2008; Aponte et al, 2009; Boja et al, 2009; Cui et al, 2010; Deng et al, 2010, 2011; Grimsrud et al, 2012; Bak et al, 2013; Zhao et al, 2011, 2014; Kruse & Højlund, 2017; Li et al, 2019; Guedouari et al, 2020; Sathe et al, 2021]). However, there has been a dramatic improvement in the technology of phosphoproteomics workflows during the last years, leading to the routine identification and quantification of thousands of phosphorylation sites in cell culture and in vivo systems (Humphrey et al, 2018; Bekker-Jensen et al, 2020) which had not been available in earlier studies. Furthermore, comparisons between mitochondrial phosphoproteomes have been difficult because only a single or a few tissues were analyzed. This complicates the combination and comparison of datasets across studies to obtain a clear view of mitochondrial diversity on proteome and phosphoproteome levels. Thus, a concerted effort is needed to systematically and quantitatively profile mitochondrial proteomes together with their matching phosphoproteomes from the same biological source. This would further help to investigate the dynamic composition of mitochondria and help identify the tissue-specific repertoire of mitochondria-resident kinases and phosphatases and their substrate associations.

Here, we performed a systematic analysis of the mitochondrial composition at the level of proteins, major functional entities, and phosphorylation in seven mouse tissues—brain, brown adipose tissue (BAT), heart, kidney, liver, skeletal muscle (SKM), and spleen. Our study employs state-of-the-art MS-based proteomics technology to systematically map divergent composition and phosphorylation of mitochondria between tissues and provides functionally valuable insights into their proteome and posttranslational regulations. This study contributes to our understanding of tissue-specific mitochondrial processes controlled by protein abundance and phosphorylation which is essential to manipulate these in health and disease. Our mitochondrial (phospho)proteomes are composed into an extensive resource and made freely accessible via mitophos.de.

Results

Comprehensive mitochondria proteome coverage across various mouse tissues

To advance our understanding of tissue-specific functional specializations of mitochondria at the protein level, we set out to characterize proteomes of mitochondria collected from various mouse tissues by LC-MS/MS analysis. To this end, we first isolated mitochondria from seven tissues—brain, BAT, heart, kidney, liver, SKM, spleen—from six 18–21-wk-old C57BL/6N mice (three females and three males). Mouse tissues were homogenized with a Dounce homogenizer, and crude mitochondria were isolated via differential centrifugation and subsequently purified on a Percoll density gradient to obtain ultra-pure mitochondria isolates (Kühl et al, 2017). Importantly, this procedure was shown to efficiently exclude contaminations from other cellular compartments (Wieckowski et al, 2009). It was possible that some of the mitochondria would lose their integrity during our multistep enrichment procedure. However, previous work using similar procedures have specifically investigated this possibility and have concluded that this is not a substantial issue (see, for example, [Becker et al, 2019] and Fig 3 from Lu et al [2022]). Furthermore, the repeated removal of contaminating material (released proteins, cytosol, cell debris, other organelles) during differential centrifugation and the concentration of largely intact mitochondria in the Percoll gradient makes a strong contamination of randomly phosphorylated/dephosphorylated mitochondria unlikely.

Proteomes of these ultra-pure mitochondrial samples were acquired by a state-of-the-art proteomics workflow (Fig 1A), allowing the robust identification and quantification (coefficient of variation [CV] < 20%) of proteins that covered a dynamic range of more than five orders of magnitude (Supplemental Data 1). In total, we identified over 7,000 proteins, of which, 1,266 were annotated as mitochondrial proteins using MitoCarta3.0 (Rath et al, 2021) and the IMPI (http://impi.mrc-mbu.cam.ac.uk/) database. This essentially covers 92% or 86% of the mitochondrial proteome by the measure of MitoCarta3.0 and the IMPI database, respectively (Fig 1B). In addition, 309 of the identified proteins were described as mitochondria-associated proteins in the IMPI database. For further analysis, we filtered for proteins identified in more than half of the biological replicates in at least one tissue, which resulted in 1,221 mitochondrial proteins. This still represents over 90% of MitoCarta3.0 and 82% of the IMPI

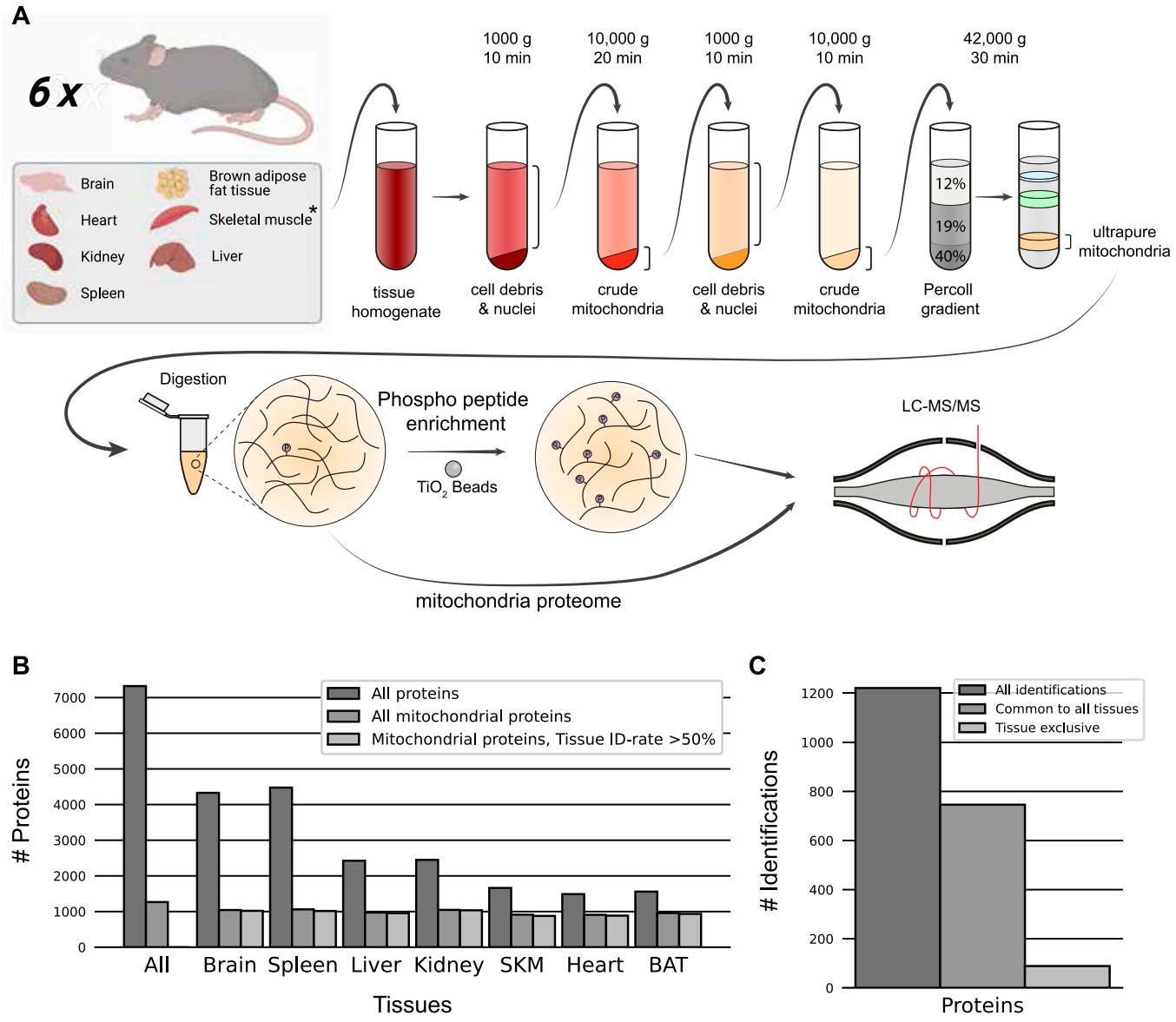

Figure 1. Mitochondrial proteome and phosphoproteome preparation.
(A) Workflow of tissue preparations for mitochondrial proteome and phosphoproteome enrichment, and LC-MS/MS analysis (n = 6). Tissues were first homogenized (* for skeletal muscle, see Materials and Methods section), crude mitochondria were isolated and ultrapure mitochondria were obtained using a Percoll gradient. Proteins were digested and prepared for phosphoproteome analysis via TiO_2 enrichment or subjected to LC-MS/MS. **(B)** Distinct protein identification across biological replicates (n = 6). Annotation of proteins as mitochondrial is based on MitoCarta3.0 and the IMPI database. **(C)** Mitochondrial protein numbers after filtering for mitochondrial proteins identified in at least 50% of biological replicates (n = 6) in at least one tissue. Skeletal muscle (SKM), brown adipose tissue (BAT).
Source data are available for this figure.

databases and highlights the deep and reproducible mitochondrial proteome coverage of this study (Fig 1C). Interestingly, more than half of these mitochondrial proteins were identified across all tissues, whereas only 7% were exclusively detected in one specific tissue (Fig 1C), confirming previous reports on mitochondrial proteomes by us and others (Mootha et al, 2003; Forner et al, 2006; Johnson et al, 2007; Calvo & Mootha, 2010). Of these, over 66% (60 proteins) were both reproducibly identified and not in the lowest 20% of ranked abundances (Supplemental Data 2), making them clear candidates for tissue-specific mitochondrial proteins. A similar proportion of the mitochondrial proteome was also exclusive to two or more tissues by the same criterion.

Mitochondrial enrichment efficiency can be determined by the proportion of summed signal intensity for mitochondrial proteins in relation to all identified proteins in measured samples (Williams et al, 2018). Applying this strategy, we determined the proportions to be very high (>90%) for liver, kidney, SKM, heart, and BAT, but lower for brain (63%) and spleen (47%) (Fig 2A). To further evaluate the mitochondrial purity, we performed a western blot analysis from sample aliquots of one mouse taken at various stages during the

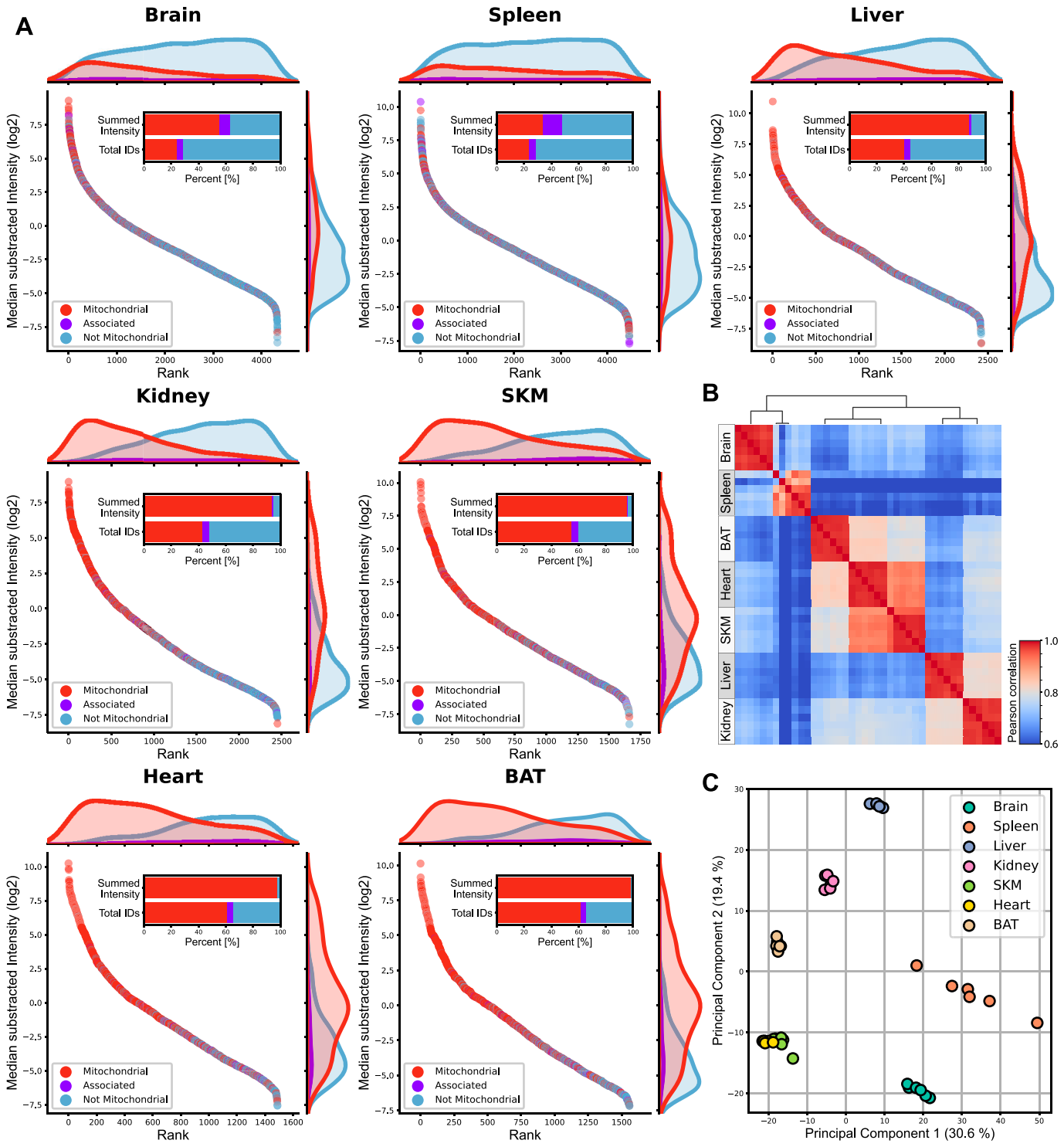

Figure 2. Mitochondria enriched samples show tissue-specific clustering.
(A) Mitochondrial (red) and not mitochondrial (blue) proteins identified, based on the MitoCarta3.0 and IMPI database, are ranked by their intensity for each individual tissue. Histograms on the top and right display the distribution of mitochondrial (red) and not mitochondrial (blue) proteins along the rank and the intensity axes, respectively. The percentage of all identified mitochondrial (red) and not mitochondrial (blue) proteins and their summed intensities are displayed in bar graphs. **(B)** Heatmap showing Pearson correlation coefficient for biological replicates (n = 6) for mitochondrial proteins of all mitochondrial enriched samples. **(C)** Principal component analysis of mitochondrial proteins of all acquired biological replicates (n = 6). Skeletal muscle (SKM), brown adipose tissue (BAT).
Source data are available for this figure.

sample preparation process (Fig S1A). This analysis is consistent with the LC-MSMS measurements and supports the effective enrichment of mitochondria within the ultrapure mitochondria fraction. The absence of the cytosolic markers tubulin or actin (for brain) in both crude and ultrapure mitochondria fractions from most tissues indicates successful reduction of cytosolic contamination (Fig S1B). However, we did detect a tubulin signal in the pure mitochondria fraction from brain tissue, which may be attributed to the known interaction between mitochondria and microtubules, particularly during processes such as axonal transport (Lewis et al, 2018). Whereas potential contamination by other cellular compartments in brain and spleen tissue cannot be completely ruled out, these trends are consistent with the established literature (Williams et al, 2018; Fecher et al, 2019; McLaughlin et al, 2020; Roberts et al, 2021) and can likely be explained by the high tissue heterogeneity of brain (Fecher et al, 2019; Menacho & Prigione, 2020) and spleen. Indeed, spleen tissue consists of various types of immune cells (Lewis et al, 2019), which might impede high purity enrichment of its organelles. For the brain, contaminations by synaptosomes, which themselves contain neuronal mitochondria, have frequently been observed (Mootha et al, 2003). Yet, correlation of both mitochondrial and all identified proteins between biological replicates yielded Pearson correlation coefficients higher than 95% in all tissues (Figs 2B and S2A). Principle component analysis further shows that biological replicates cluster together and underlines functional similarities between tissues such as heart and SKM and tissue-related diversity of mitochondria proteomes (Figs 2C and S2B).

Mitochondrial proteome composition reveals tissue-specific functions

To gain further insights into tissue-specific functional differences in mitochondria, we investigated differences in the composition of mitochondrial proteomes across tissues. First, we focused on the oxidative phosphorylation system, which is essential for production of the energy-rich metabolite ATP and other processes like free radical generation and apoptosis (Hüttemann et al, 2007). We found that proteins of the electron transport chain (Complex I–Complex IV) and ATP-synthase (Complex V) displayed high abundances in heart and SKM tissues, supporting the physiological requirement of high ATP levels in both muscular tissues to sustain processes like muscle contraction (Ferreira et al, 2010; Ventura-Clapier et al, 2011) (Fig 3A). Conversely, levels of Complex V proteins were substantially lower in mitochondria from BAT compared with all other measured tissues (Fig 3A), which agrees with the specialized function of BAT in non-shivering thermogenesis (Jastroch et al, 2010; Kajimura & Saito, 2014; Oelkrug et al, 2015). This was further supported by the high abundance of the uncoupling protein 1 in our proteome measurements, the key mediator of the heat-generating proton leak in the mitochondria of BAT (Fig 3B).

In contrast to the well-described uncoupling protein 1, several other members of the SLC25 family remain uncharacterized (Ruprecht & Kunji, 2020). In our dataset, we identified a total of 47 members of the SLC25 family (Kunji et al, 2020). We found that levels of SLC25A23 and SLC25A25, two ATP-Mg^{2+}/P_i carrier paralogues, (del Arco & Satrustegui, 2004; Fiermonte et al, 2004), displayed high abundance in the mitochondria of brain tissue (Fig 3C and D). Interestingly, knockout of SLC25A23 was shown to increase neuronal vulnerability (Rueda et al, 2015), which corroborates our observation and suggests an important role of SLC25A25 in this tissue type. We also quantified a third paralogue, SLC25A24, which showed a higher abundance in spleen tissue. Notably, the spleen harbors a large pool of B-cells and reduced SLC25A24 levels were previously linked to B-cell malignancies (Sandhu et al, 2013) (Fig 3E). Although these three ATP-Mg^{2+}/P_i carriers were not detected in the mitochondria from heart tissue, we identified another class of ATP carriers, including SLC25A4 or SLC25A31, which both showed increased abundance in the heart compared with all other measured tissues. Such differences between mitochondrial proteome compositions are easily retrieved from our dataset, facilitating a better understanding of mitochondrial plasticity across tissues.

Tissue specificity of mitochondria-associated proteins

The identification of key proteins mediating the crosstalk of mitochondria with their cellular environment is crucial to better understand their tissue-specific regulation and this concept has already attracted considerable interest in recent years (Montes de Oca Balderas, 2021). Although the characterization of local proteomes of organellar contact sites usually requires special centrifugation-based isolation methods, we anticipated that a considerable fraction of mitochondria-associated proteins would also enrich along with the mitochondria in our samples. We first performed an annotation term enrichment analysis of all identified proteins. Whereas we observed significant enrichment of several mitochondria related terms in all tissues as expected, the non-mitochondrial protein pool was largely enriched for terms related to the tissue of origin (Fig S3, SourceDataForFigure4). For instance, terms like "positive regulation of B cell activation" in spleen or "positive regulation of synapse assembly" in brain tissue suggest tissue-specific functions. The enrichment of G-protein associated terms marks an exception, as these were enriched across all tested tissues.

Next, we performed a network analysis to evaluate the nature and quality of co-enriched proteins, more specifically whether non-mitochondrial proteins identified in these samples are associating proteins with functional roles or biological contaminations that are likely tissue-specific and highly abundant. This analysis revealed several clusters of known mitochondrial complexes such as the TIM23 complex or processes like the ubiquinone biosynthetic process, whose members were robustly identified in all tissues, and several clusters including both mitochondrial and non-mitochondrial proteins (Fig 4). For instance, one cluster consisted of G proteins, some of which were identified throughout all tissues and shown to localize to mitochondria (e.g., GNAI2) (Benincá et al, 2014), although not annotated as mitochondrial proteins by the IMPI or MitoCarta3.0 database. Interestingly, like most of the proteins in the G protein cluster, many G-protein–coupled receptors were exclusively identified in brain tissue. A prominent member of these brain-specific G protein coupled receptors is CNR1, which was reported to localize to mitochondria where it plays an important role in the regulation of memory processes through the modulation of the mitochondrial energy metabolism (Hebert-Chatelain et al, 2016). These examples underscore the

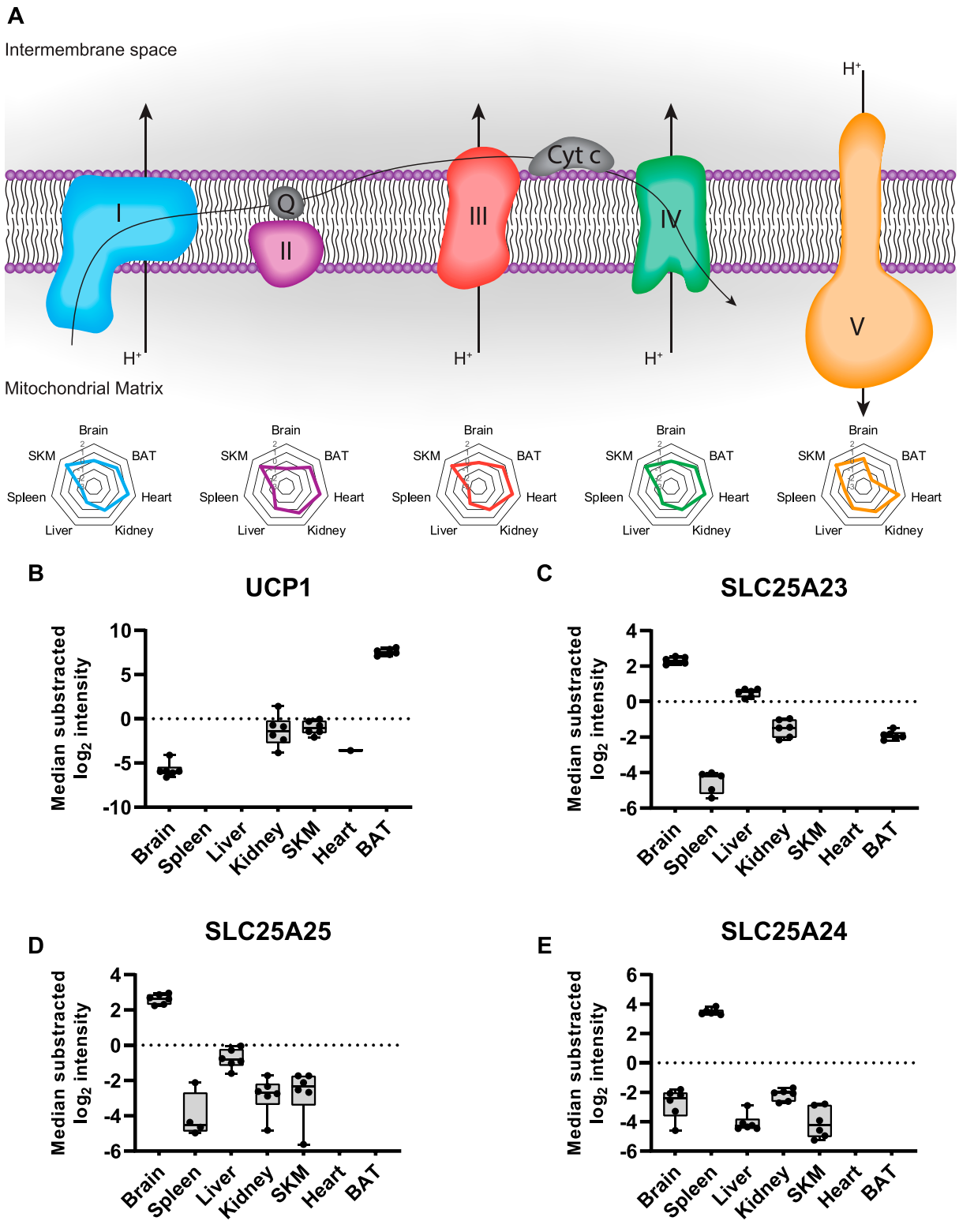

Figure 3. Tissue-specific protein contribution of SLC25 proteins the mitochondrial proteome.
(A) Representation of the oxidative phosphorylation system including from left to right the electron transport chain (Complex I [blue], Complex II [violet], Complex III [red], Complex IV [green]), and ATP synthase (Complex V [yellow]). Radar plots show the relative contribution of the corresponding complex across the analyzed tissues to the overall mitochondrial composition (see Materials and Methods section for detailed description). **(B, C, D, E)** Normalized intensity (median of all $\log_2$ transformed mitochondrial proteins of a sample was subtracted from all $\log_2$ protein intensities of that sample) of the uncoupling protein 1 (UCP1), (C) SLC25A23, (D) SLC25A25, and (E) SLC25A24 across all analyzed tissues (black dots indicate individual identifications). **(B, C, D, E)** Protein abundance differences in relation to the reference tissue (BAT in

potential of our dataset in facilitating the identification of previously unrecognized mitochondrial and mitochondria-associated proteins through a hypothesis-free approach. Another cluster consisting of mitochondrial and non-mitochondrial proteins contains enzymes of the kynurenine pathway involved in the catabolism of tryptophan. Similar to the mitochondrial transaminases, Ccbl2 and Aadat, Ccbl1 was identified throughout all tissues (Han et al, 2010). Interestingly, Ccbl1 has a cytosolic and a mitochondrial isoform and has been previously shown to localize to the mitochondrial matrix (Malherbe et al, 1995).

Mitochondrial kinases and phosphatases show tissue specificity

Posttranslational modification of proteins, specifically phosphorylation, plays a crucial role in the orchestration of mitochondrial protein function (Niemi & Pagliarini, 2021). However, almost no mitochondrial kinases with mitochondrial targeting sequences have been consistently reported and most kinases shown to associate with mitochondria have been found on or interact with the outer membrane (Kotrasová et al, 2021). Given our deep mitochondrial proteomes, we investigated relative abundances of kinases and phosphatases, which are annotated as or suggested to be mitochondrial, across mouse tissues. Note, however, that this includes Adcks and Fastk, which have recently been suggested to not be bona fide kinases (Stefely et al, 2016; Jourdain et al, 2017).

Firstly, we observed clear differences in abundances of identified mitochondrial kinases and phosphatases, including well-described matrix kinases and phosphatases, between tissues (Fig 5A). For instance, PDK1, PDK2, and PDK4 contributed preferentially to the composition of heart, SKM, and BAT mitochondria, whereas the PDK3 was more abundant in brain, spleen, and kidney mitochondria (Fig S4A). These tissue-related differences are in line with earlier reports and suggest a specialized function of PDK3, which may originate in its insensitivity to pyruvate inhibition (Sadana et al, 2018; Klyuyeva et al, 2019). Similarly, levels of the heterodimeric pyruvate dehydrogenase phosphatase consisting of PDP1 and PDPr were elevated in brain, SKM, and heart compared with the remaining tissues, whereas PDP2 contributes more to the composition of liver, kidney, and BAT mitochondria (Fig S4B). Although our study confirmed previous reports on the differential expressions of these proteins in a tissue-specific manner (Huang et al, 1998, 2003), it also provided quantitative data to assess the magnitude of these differences. We detected more kinases in brain and spleen tissues compared with the other tissues. This observation may reflect inherent tissue heterogeneity—for instance, its many different cell types. It could also be attributable to reduced mitochondrial purity in these particular tissue samples, as reflected in the higher proportion of MS signal from non-mitochondrial proteins. Together, our results imply a tailored regulation of kinase and phosphatase abundances across tissues to modulate the mitochondrial phosphoproteome.

To investigate if and how kinase and phosphatase levels translate into protein phosphorylation, we analyzed the mitochondrial phosphoproteomes of the same samples collected from all seven tissues (Fig 1A). As always in phosphoproteomics, disruption of the cellular environment could expose substrates to unphysiological kinases or phosphatases, although we do not see any evidence of this in our protocol. Our analysis resulted in the identification of 991 phosphorylation sites on 474 mitochondrial proteins and 361 phosphorylation sites on 163 mitochondria-associated proteins (Fig 5B, SourceDataForFigure5). After stringent filtering of the data for more than four identifications across six biological replicates in at least one tissue and a site localization score higher than 75%, we obtained a dataset of 618 phosphorylation sites on 335 mitochondrial proteins (Fig 5C, SourceDataForFigure5). Of these high-confidence sites, 16% have previously not been reported in mice according to the PhosphoSitePlus database (Hornbeck et al, 2012). Strikingly, in contrast to the mitochondrial proteomes, 32% of the phosphosites identified on mitochondrial proteins were exclusive to one tissue, and only 9% were identified in all the tissues measured (Fig 5C). This might indicate that mitochondrial diversity is more strongly pronounced at the phosphorylation than the protein level.

Next, we investigated whether there exists a correlation between the abundances of kinases and their documented phosphorylation sites across various tissues. The aforementioned PDK kinases were previously reported to regulate the phosphorylation of the phosphorylation sites S293, S300, and S232 on PDHA1 (Korotchkina & Patel, 2001). These authors further showed that PDK1 is predominantly responsible for the phosphorylation of S232 on PDHA1. In our data, there was no clear correlation between the kinase and its respective phosphorylation site (Fig S4C). The absence of a definitive link between PDK1 and S232 phosphorylation abundance in our dataset suggests the need to consider additional factors like signaling events or phosphatase activity across different tissues to comprehensively evaluate the phosphorylation status of distinct phosphosites. For instance, the phosphatases PDP1 and PDP2 measured here by proteomics both have the capability to dephosphorylate S293, S300, and S232 on PDHA1, albeit with varying efficiencies (Karpova et al, 2003).

Another example for a known phosphatase—substrate relation exists between the phosphatase Pptc7 and the phosphorylation of T33 on Timm50 (Niemi et al, 2019). Although excluded by our stringent filtering criteria that require the presence of a phosphorylation site in five of six replicates, it is interesting to note that we observe low Pptc7 levels in liver, which is the only tissue where we detect Timm50 T33 phosphorylation, congruent with the phosphatase—substrate relationship.

Mitochondrial phosphoproteomes exhibit extensive intra-mitochondrial phosphorylation

To understand the distribution of mitochondrial phosphoproteins across mitochondrial compartments, we examined the sub-mitochondrial localization based on the curated MitoCarta3.0

(B), brain in (C, D) and spleen in (E)) were significant (P-value < 0.0001) by one-way ANOVA analysis (SourceDataForFigure3). Data in this figure are based on the analysis of six replicates (n = 6) for each tissue. Skeletal muscle (SKM), brown adipose tissue (BAT).
Source data are available for this figure.

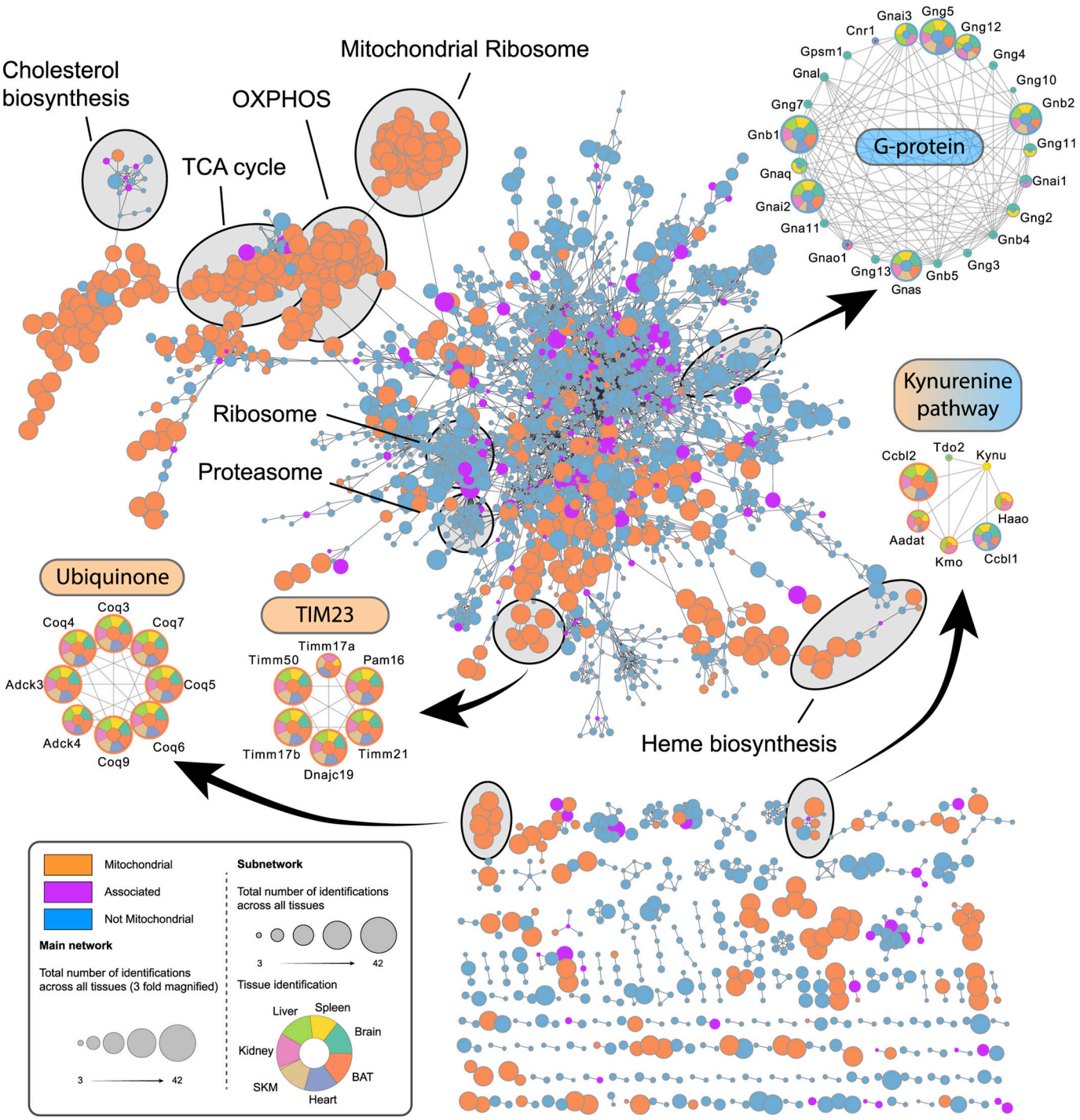

Figure 4. Proteome of mitochondria enriched samples displays tissue-specific complexes.
Cytoscape network analysis of reproducibly (>50% identification rate in at least one tissue, six replicates were analyzed [n = 6]) identified proteins of all mitochondria enriched samples. The main network depicts mitochondrial (orange) and non-mitochondrial (blue) proteins with at least one edge (String score >0.95). The size of individual nodes represents the number of identifications ranging from 3 (small circle) to 42 (big circle). Subnetworks display mitochondrial (orange) and non-mitochondrial (blue) proteins and tissues in which they were identified (dark green—brain; yellow—spleen; light green—liver; pink—kidney; ochre—SKM; blue—heart; orange—BAT). Skeletal muscle (SKM), brown adipose tissue (BAT).
Source data are available for this figure.

annotation. Mitochondria are typically divided into four main compartments, that is, mitochondrial outer membrane (OMM), intermembrane space, inner mitochondrial membrane (IMM), and matrix, although the complex organization of the IMM possibly may define additional compartments (Colina-Tenorio et al, 2020). In line with the high proportion of shared mitochondrial

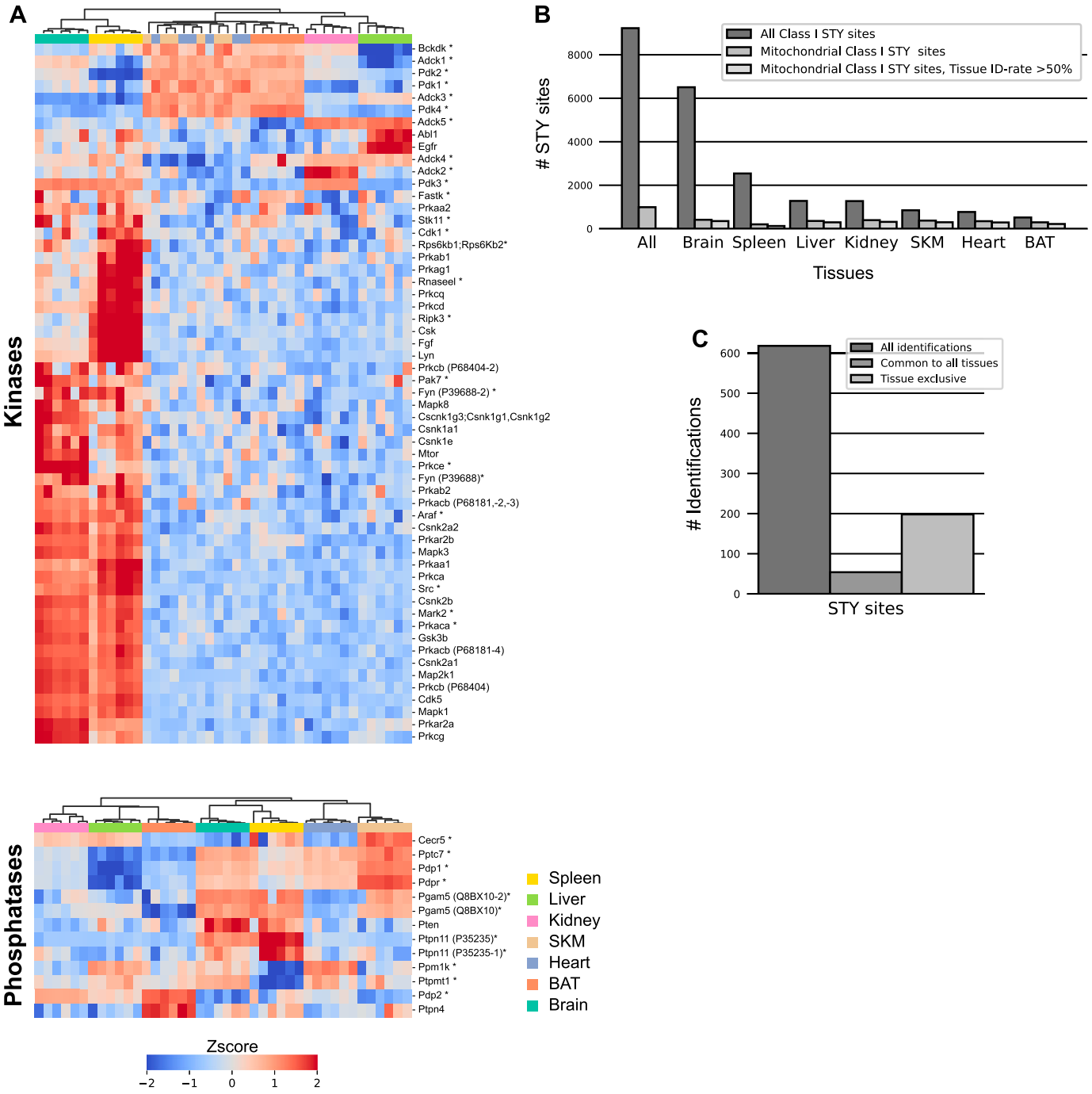

Figure 5. Tissue specificity of mitochondrial kinases and phosphatases.
(A) Z-scored protein abundances for predicted (triangle), known (star) (based on MitoCarta3.0 and IMPI database), and manually curated (SourceDataForFigure5) mitochondrial kinases (top) and phosphatases (bottom) across analyzed tissues. Skeletal muscle (SKM), brown adipose tissue (BAT). **(B)** STY site identification numbers. **(C)** Mitochondrial STY site numbers after filtering for mitochondrial STY sites identified in at least five out of six biological replicates in one tissue. Identification numbers for all identified STY sites (left), STY sites common to all tissues (middle), and STY sites exclusive to one tissue (right) are shown. Data in this figure are based on the analysis of six replicates (n = 6) for each tissue. Skeletal muscle (SKM), brown adipose tissue (BAT).
Source data are available for this figure.

proteomes across all tissues (Fig 1C), the overall localization of proteins was not different between tissues and closely resembled the distribution of all annotated mitochondrial proteins in the database (Fig 6A). However, when performing the same analysis using the phosphorylated mitochondrial proteins, we observed a significant shift towards a localization to the OMM in all tissues (adj. *P*-values < 1.6×10^{-9}) (Figs 6A and S5). Surprisingly, our data also showed that depending on the tissue type, more than

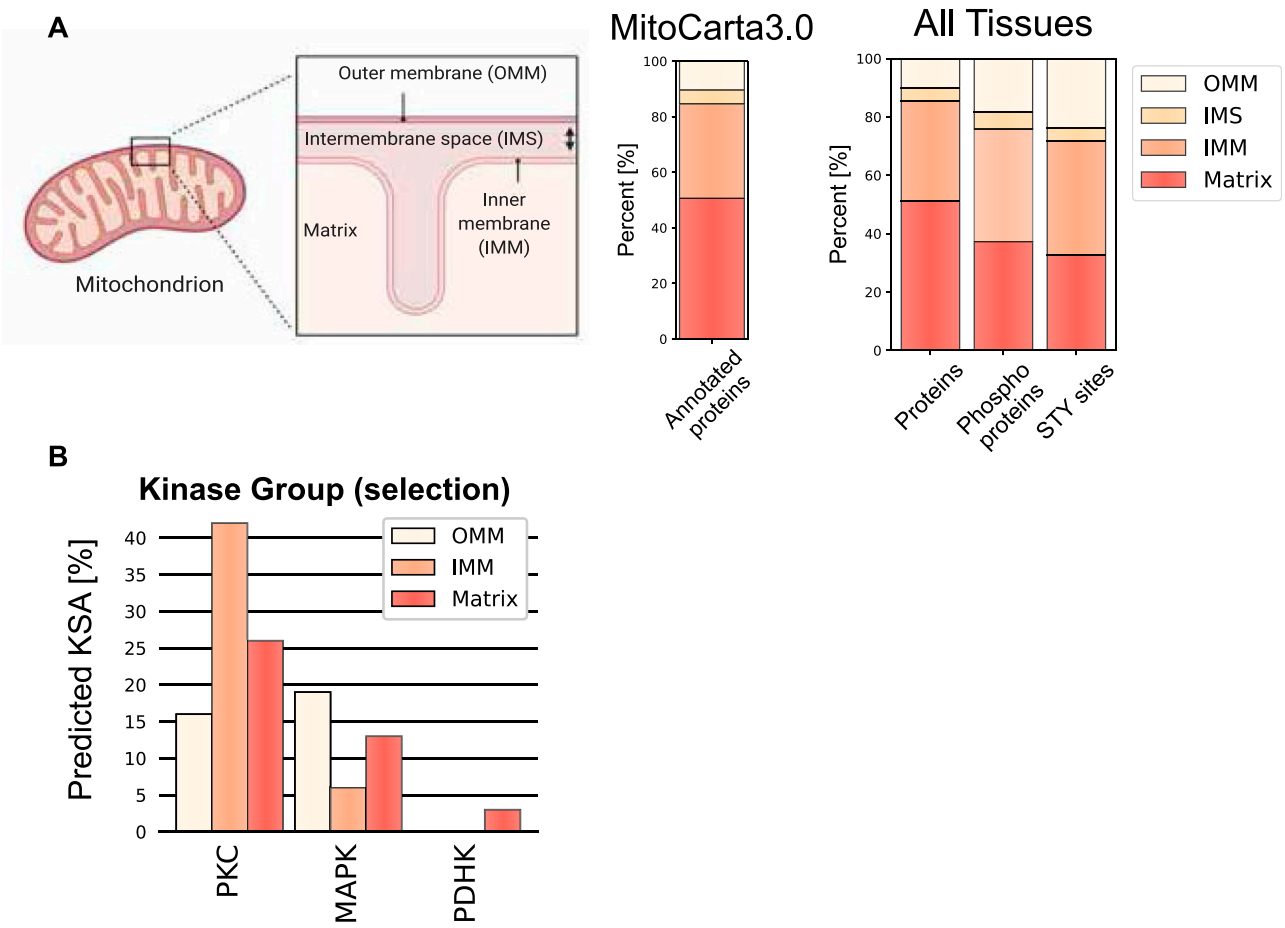

Figure 6. Localization distribution of mitochondrial phosphoproteome diverges from mitochondrial proteome.
(A) Simplified scheme of a mitochondrion with four different mitochondrial localizations—outer mitochondrial membrane, intermembrane space, inner mitochondrial membrane, matrix—and the distribution of mitochondrial proteins contained in and classified by the MitoCarta3.0 database. Bar graphs show the precentral distribution of mitochondrial proteins (left), phosphoproteins (middle), and STY sites (right) across different mitochondrial localizations. **(B)** Predicted kinase substrate associations by the NetworKin3.0 tool for selected kinase families. Data in this figure are based on the analysis of six replicates for seven different tissues.
Source data are available for this figure.

60% of phosphorylated mitochondrial proteins had an intra-mitochondrial annotation—IMM, intermembrane space or matrix localization—(Figs 6A and S5). Interestingly, 23–50% of OMM, but only 3–21% of intra-mitochondrial proteins was phosphorylated. Here, especially brain (8%) and spleen (4%) tissues showed low intramitochondrial phosphorylation rates. Given their unique evolutionary origins, we were interested in phosphorylation sites on proteins encoded by mitochondrial DNA, but failed to detect any (Table S2).

We further investigated the localization of specific kinase-substrate associations (KSA) across sub-mitochondrial localizations using NetworKin3.0 (Horn et al, 2014). Prominently, more than 40% of the predicted KSA in the IMM were linked to the PKC kinase family (Fig 6B). Studies have already reported the localization of PKC kinase family members to mitochondria, and an increased phosphorylation of the IMM protein COX IV after PKCε activation (Majumder et al, 2000; Baines et al, 2002; Ping et al, 2002; Jaburek et al, 2006; Ogbi & Johnson, 2006). Moreover, the MAPK group appeared to act on proteins localized to the OMM and matrix, whereas the PDHK family (including PDHK1–4 and Bckdk) was specifically associated with the matrix proteins (Fig 6B). The members of the latter kinase family are known to localize to the mitochondria matrix (Hitosugi et al, 2011), further supporting the validity of identified KSA. However, molecular studies are needed to investigate such KSA, whether phosphorylation of intra-mitochondrial proteins occurs in situ or outside mitochondria before being imported into mitochondria, how and which kinases/phosphatases translocate to or into mitochondria, and whether these phosphorylation events are functionally relevant.

Mitochondrial phosphoproteome reveals tissue-specific modulation of fusion and fission events

The tissue-specific phosphorylation of mitochondrial proteins suggested functional differences in mitochondria and prompted us to investigate the influence of phosphorylation on mitochondrial dynamics. We focused on proteins involved in mitochondrial fusion and fission, two important counteracting events involved in

organelle distribution, size balancing, and maintenance of a healthy mitochondrial network (Silva Ramos et al, 2019; Liu et al, 2020). Especially proteins involved in the fission process are regulated by a range of protein modifications, including phosphorylation (Cribbs & Strack, 2007; Taguchi et al, 2007; van der Bliek et al, 2013).

Throughout all tissues, MIGA1 (FAM73A) and MIGA2 (FAM73B), two homologues regulating mitochondrial fusion by functioning downstream of the mitofusins, showed different abundances (Fig S6). This is especially interesting because MIGA1 and MIGA2 can form hetero and homodimers, highlighting a different regulation of fusion in different tissues (Zhang et al, 2016). Moreover, we identified multiple phosphorylation site clusters on MIGA2, whereas none were identified on MIGA1 (Fig S6). Intriguingly, similar phosphorylation clusters were identified on Miga in *Drosophila melanogaster* (Xu et al, 2020). Interestingly, two phosphorylation sites on Miga, S246 and S249, were reported to be essential for Vap33 interaction and the establishment of endoplasmic reticulum–mitochondria contact site (ERMCS), suggesting that phosphorylation on MIGA2 has similar functions in mammals (Xu et al, 2020).

Moreover, we observed that GTPase dynamin-related protein 1 (DRP1), a crucial player initiating mitochondrial fission (Bleazard et al, 1999; Cereghetti et al, 2008), displayed higher abundance in brain compared with other tissues (Fig 7A). This observation supports the importance of mitochondrial fission in neurons, where mitochondria switch to a fragmented morphology to enter and travel through axons (Lewis et al, 2018). We cannot exclude that the signal for DRP1 could be related to the lower mitochondrial purity in brain tissue. However, increased levels of serine 622 phosphorylation on DRP1, a site that has been shown to regulate DRP1 translocation to mitochondria (Cribbs & Strack, 2007; Taguchi et al, 2007; Cereghetti et al, 2008), suggests that DRP1 is actively localized to mitochondria, likely to regulate frequent fission events in the brain tissue (Fig 7B). Furthermore, we detected Erk2, a kinase capable of phosphorylating DRP1 at S622 (Kashatus et al, 2015), in both brain and spleen tissues (Fig S7A). Intriguingly, we also observed phosphorylation of Erk2 at residues T183 and Y185, sites known to be associated with the mitochondrial localization of Erk2 (Fig S7B) (Helfenberger et al, 2018).

In mammals, four DRP1 receptor proteins, that are all integral membrane proteins of the OMM, have been reported: mitochondrial fission protein 1 (FIS1), mitochondrial fission factor (MFF), and mitochondrial dynamics protein MiD49 (MIEF1) and MiD51 (MIEF2) (Losón et al, 2013). MFF and FIS1, the fission-promoting receptors, were robustly quantified in all tissues and displayed higher abundances in brain and spleen compared with other tissues (Fig 7A). However, MIEF1/2, which counteract DRP1-mediated fission (Dikov & Reichert, 2011; Liu et al, 2013), were generally too low to be robustly quantified in the measured tissues. In addition, we detected higher levels of MFF phosphorylation at the serine 129 and 146 residues in brain tissue compared with all other tissues in which they were detected (Fig 7C and D). Both sites are essential for the recruitment of DRP1 and initiation of fission (Ducommun et al, 2015; Toyama et al, 2016; Lewis et al, 2018).

Elevated DRP1 levels have been shown to increase reactive oxygen species levels (Watanabe et al, 2014). Intriguingly, we identified oxidation resistance 1 (OXR1), exclusively in the mitochondria of brain tissue, where it plays an important role in the protection of neuronal cells from oxidative stress (Volkert & Crowley, 2020). This likely indicates a protective function of OXR1 in brain tissue as a response to the prevalent fragmented organellar morphology induced by DRP1. In addition, we found OXR1 to be hyperphosphorylated and three out of 12 high-confidence sites were novel (Fig 7E). Tissue specificity and the lack of functional annotation of phosphorylation sites that are identified in our study make OXR1 an exciting candidate to be investigated in the future.

Web application makes Mouse Mitochondria Atlas data readily accessible

As indicated by the above examples, this study presents a rich resource to explore the mitochondrial proteomes and phosphoproteomes across mouse tissues. Preceding examples show the potential of this resource for investigation of tissue-specific mitochondrial regulations on the proteome and phosphoproteome levels, ultimately permitting the generation and analysis of new hypotheses. However, use of such resources largely depends on the ease of data access for exploration.

To this end, we created a web application mitophos.de offering the end user an interface to easily explore datasets, including MitoCarta3.0 networks, abundance comparisons across tissues, and sequence analysis (Fig 8A). As an example, Fig 8 illustrates the MICOS complex, which has a central role in mitochondria (Khosravi & Harner, 2020). In the network view, one can see (I) members of the complex and the phosphorylation sites identified on these proteins and (II) in which tissues and how reproducibly they are identified in our dataset (Fig 8B). Moreover, the user can inspect individual abundance distributions of all identified proteins/STY sites across all measured tissues. For instance, MINOS1, a core component of the MICOS complex (Bohnert et al, 2015), displayed high abundance in mitochondria isolated from heart, SKM, and BAT tissues (Fig 8C). Moreover, in the sequence view the AlphaMap tool (Voytik et al, 2022) is integrated to map all identified peptides, including phosphorylated peptides, onto their respective protein sequence along with structural information such as topological domains and transmembrane regions (Fig 8D) and to visualize phosphorylation sites in their 3D structures (unpublished data) as predicted by AlphaFold (Jumper et al, 2021).

Together, this data-rich and comprehensive tool is an entry point to investigate the herein presented resource and will assist in future efforts to functionally characterize mitochondrial proteins and their respective phosphorylation sites.

Discussion

Here, we present a tissue-specific atlas of mouse mitochondrial proteomes and phosphoproteomes, an in-depth resource towards a better understanding of the composition and function of this vital organelle in a tissue-specific manner. Previous MS-based studies combining mitochondrial phosphoproteome and proteome measurements typically focused on a single or few tissues and were generally shallower than our study. In addition,

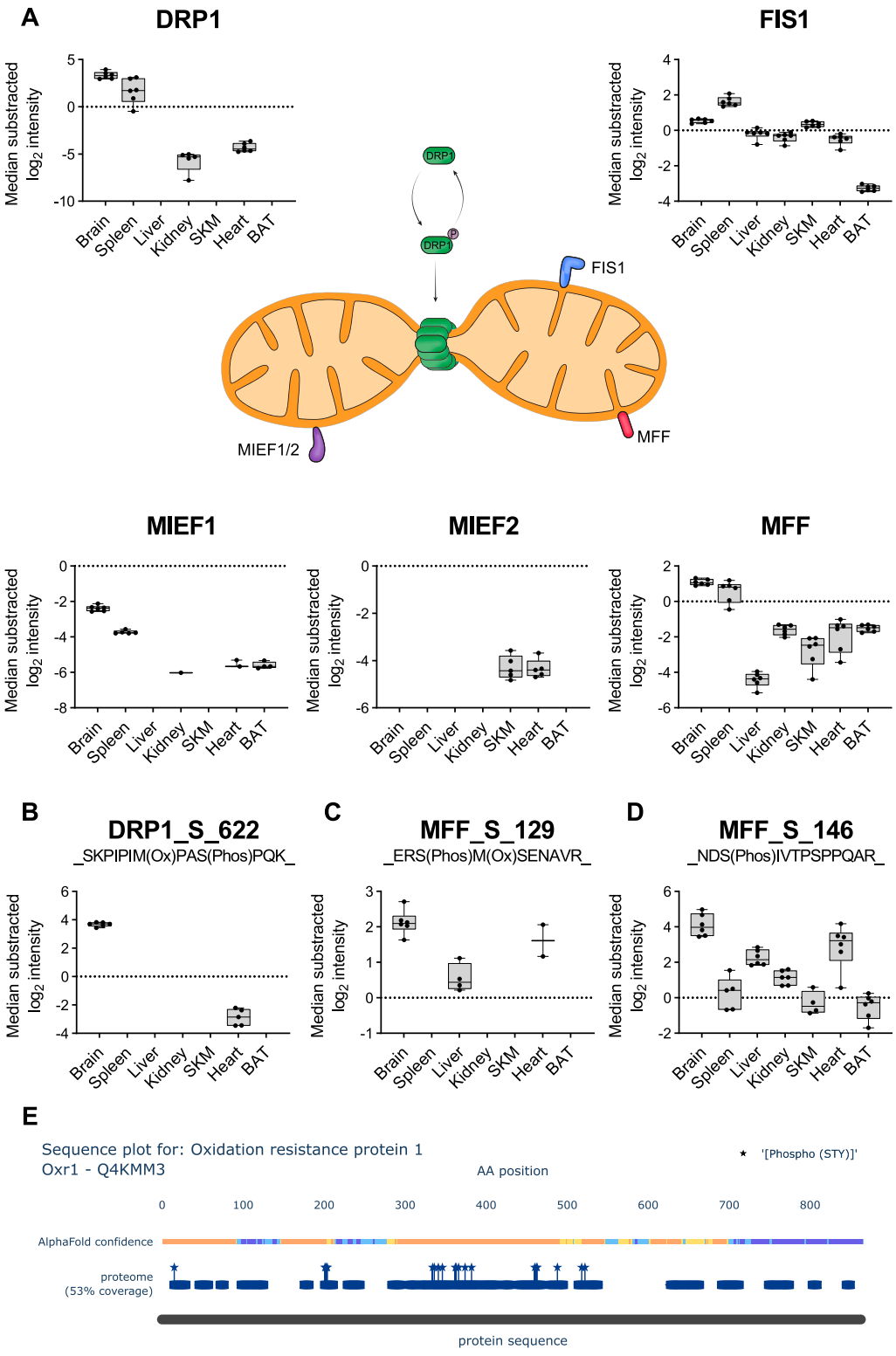

Figure 7. Phosphoproteome reveals tissue-specific functionality for mitochondrial fission.
(A) Scheme displays the reversible phosphorylation and the connected localization change to mitochondria of dynamin-related protein 1 (DRP1) (green). Normalized intensities (median of all $\log_2$ transformed mitochondrial proteins of a sample was subtracted from all $\log_2$ protein intensities of that sample) of DRP1 across all analyzed tissues (black dots indicate individual identifications) are displayed in the upper left. Mitochondrial DRP1 receptors—FIS1 (blue), MIEF1/2 (violet), mitochondrial fission factor (MFF) (red)—and corresponding box plots are shown next to their receptors. **(B)** Normalized intensities (median of all $\log_2$ transformed mitochondrial phosphopeptide of a sample was subtracted from all $\log_2$ peptide intensities of that sample) of the phosphopeptide showing S622 phosphorylation on DRP1 (black dots indicate individual identifications). **(C)** Same as (B) showing S129 phosphorylation on MFF. **(D)** Same as (B) showing S146 phosphorylation on MFF. Significance of protein abundance differences in relation to the reference tissue (brain for DRP1 panel, brain and spleen in FIS1 and MFF panels) were estimated (*P*-values < 0.001, except for SKM in FIS1 panel) by one-way ANOVA analysis (SourceDataForFigure7). **(B, C)** Significance of phosphosite abundance differences in (B) and ((C), only brain and liver) were estimated by a two-side *t* test (SourceDataForFigure7). Significance of MFF_S_146 abundance differences in relation to the reference tissue (brain) were estimated (*P*-value < 0.05) by one-way ANOVA analysis (SourceDataForFigure7). **(E)** Sequence plot of oxidation resistance 1 shows structural information (based on UniProt annotations) and protein coverage based on identified peptides. All identified STY sites are marked with a star. Data in this figure are based on the analysis of six replicates (n = 6). Skeletal muscle (SKM), brown adipose tissue (BAT). Source data are available for this figure.

differences in study designs such as the use of various organisms or mitochondria/phosphopeptide enrichment protocols, analysis pipelines, and mitochondrial protein annotation databases, complicate the integration of such datasets to understand tissue specificity. We now globally and precisely quantified different protein expression and phosphorylation patterns at subcellular level across seven mouse tissues, providing a detailed view on mitochondrial diversity. The breadth and depth of coverage achieved

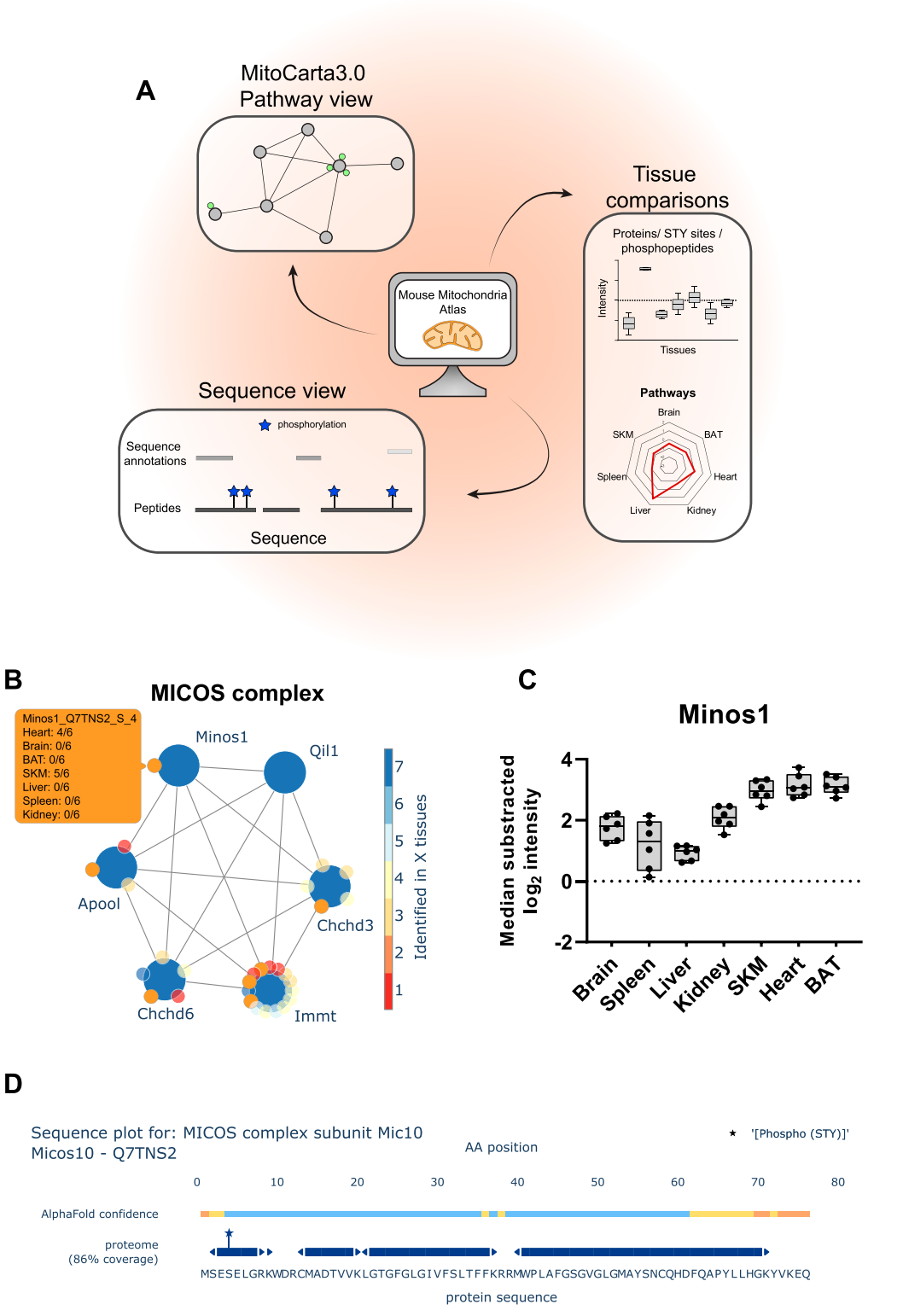

Figure 8. Web application readily enables easy data access.
(A) Scheme of Mouse Mitochondria Atlas application features (mitophos.de). **(B)** MICOS complex view based on MitoCarta3.0 annotation. Large and small nodes represent proteins and class I STY sites, respectively. Edges represent on String interaction scores >0.4 and color of nodes indicate the number of tissues in which proteins/STY sites were identified. **(C)** Normalized intensities (median of all $\log_2$ transformed mitochondrial proteins of a sample was subtracted from all $\log_2$ protein intensities of that sample) for Minos1 across all analyzed tissues (black dots indicate individual identifications, box and error bar). **(D)** Sequence plot of Micos1 shows structural information (based on UniProt annotations) and protein coverage based on identified peptides. All identified STY sites are marked with a star. Data in this figure are based on the analysis of six replicates (n = 6). Skeletal muscle (SKM), brown adipose tissue (BAT).

by the integration of tissue-specific mitochondrial proteomes and phosphoproteomes provide unbiased insights into the mitochondrial composition and function. This allows the generation and assessment of novel hypotheses related to mitochondrial biology, which cannot be generated with focused studies alone. Integrated mitochondrial proteomes and phosphoproteomes that are diverse between tissues can readily be explored at mitophos.de.

Our data revealed that the functional diversity of mitochondria is defined by protein abundance rather than compositional differences because more than half of the mitochondrial proteome was shared by all analyzed tissues and 90% by at least two tissues. For instance, the electron transport chain is an integral part of the mitochondrial composition and its components are found across all tissues; however, their abundance shows substantial differences to meet tissue-specific energy demands. Thus, dysregulation of individual proteins can strongly affect mitochondria in one tissue, leading to severe diseases, whereas mitochondria in a different tissue remain largely unaffected. Moreover, we found that 7% of the proteome displays tissue specificity, further contributing to our understanding of tissue-specific effects of mitochondrial protein dysregulation (Russell et al, 2020). This is an important concept, which can now be studied in an unbiased manner using our resource data, providing opportunities for development of targeted treatments for mitochondrial diseases. For instance, members of the SLC25 family are linked to metabolic diseases in distinct tissues (Palmieri & Monne, 2016) and various cancers (Rochette et al, 2020). However, biological functions of a large repertoire of mitochondrial SLCs are still unknown. For example, inactivation of SLC25A25 was assessed in mouse SKM tissue where it caused a reduced metabolic efficiency (Anunciado-Koza et al, 2011). Given its high abundance in the mitochondria of brain tissue and in glioma cells (Traba et al, 2012), it will also be interesting to investigate its role in this tissue, particularly whether SLC25A25 deficiency influences neuronal fitness.

Mitochondria are essential cellular entities that are involved in a wide variety of cellular processes (McBride et al, 2006) through dynamic interaction and constant communication with other organelles such as the (ER), nucleus, and peroxisomes via membrane contact sites (Shai et al, 2018; Desai et al, 2020; Perrone et al, 2020) or protein complexes, such as the ribosome (Lashkevich & Dmitriev, 2021). We suggest that non-mitochondrial proteins identified in the samples might present signatures that could convey important biological information regarding mitochondria-associated structures. Given the high level of mitochondrial enrichment combined with highly reproducible LC-MS/MS measurements, such protein signatures are unlikely to be solely based on unspecific enrichment of abundant proteins. For example, the proteasome is robustly identified in most of the mitochondria-enriched samples, which is in line with its involvement in the degradation of misfolded mitochondrial proteins (Basch et al, 2020; Kodron et al, 2021). We also observed multiple G-proteins that were previously shown to interact with mitochondria, demonstrating the relevance of mitochondria in cellular signaling processes. Furthermore, our data identified non-mitochondrial ribosomal proteins in all tissues, which could be explained by the local translation of nuclear-encoded mitochondrial mRNAs (Lashkevich & Dmitriev, 2021). It was recently shown that RNA-bearing late endosomes associate with mitochondria and ribosomes forming hotspots of local protein synthesis in axons (Cioni et al, 2019) and that mitochondria fuel such local translations in neurons, enabling synaptic plasticity (Rangaraju et al, 2019).

There is mounting evidence that phosphorylation of mitochondrial proteins fulfills important functions to maintain cellular health as exemplified by the fission process in this study. Deregulation of mitochondrial protein phosphorylation can lead to diseases such as cancer, diabetes, heart and neurological disorders. It was recently reported that 91% of mitochondrial proteins on MitoCarta3.0 have at least one phosphorylation site reported on the PhosphoSitePlus database (Niemi & Pagliarini, 2021). However, this analysis also includes proteins that do not always localize to mitochondria (Ben-Menachem et al, 2011) and phosphorylation sites that can specifically be captured upon perturbations and stimuli. Our study revealed that around one third of the mitochondria-localized proteins were phosphorylated in tissues at steady state. This suggests that the mitochondrial proteome and phosphoproteome compositions are dynamically modulated in response to environmental changes. Furthermore, we identified 57 kinases and 11 phosphatases that either are localized to mitochondria or associate with mitochondria, providing a global view on important modulators of mitochondrial protein phosphorylation. Mapping tissue-specific mitochondrial kinases and phosphatases is an important step towards understanding their role in the regulation of the mitochondrial phosphoproteome in different tissues and hence developing therapeutics for mitochondrial diseases. For example, a mitochondrial phosphatase, phosphoglycerate mutase family member 5 (PGAM5), has recently emerged as an important regulator of mitochondrial homeostasis. Deletion of PGAM5 has been shown to result in Parkinson's-like movement disorder in mice (Lu et al, 2014) and T cell dysfunction in primary cells (Panda et al, 2016). Although its diverse roles largely remain to be uncovered (Liang et al, 2021), a novel PGAM5 inhibitor was recently suggested as a potential therapeutic for brain ischemic stroke (Gao et al, 2021). We observed that PGAM5 displays elevated levels in the mitochondria isolated from brain, SKM, and spleen, possibly explaining the tissue-specific phenotypes induced by its absence and where in the body molecules targeting its phosphatase activity would exert their effects.

The data in this study will contribute to our understanding of the tissue-specific composition and function of mitochondria and serve as a gateway for investigation of specific questions related to mitochondrial biology. Future biochemical and more focused investigations are needed to validate our findings and test the hypotheses arising from our study. For instance, it is pivotal to experimentally validate KSA of previously unknown phosphorylations on mitochondrial proteins and their functional implications in the cell. In addition, the impact of those phosphorylations on the localization of target proteins and, more specifically, the question of whether mitochondrial proteins are phosphorylated before or after entering the mitochondria remain to be investigated. Accessibility, for instance, of previously undescribed phosphorylation sites on mitochondrial proteins can be assessed using advanced structural tools (Jumper et al, 2021) to determine if they are likely targeted by a mitochondrial kinase or a

cytoplasmic kinase before being imported (Rosenberger et al, 2021). Moreover, future developments towards better enrichment strategies for the isolation of mitochondria from different tissues and advances in the MS technology will aid to further improve the depth and quality of the mitochondrial proteomes and phosphoproteome.

Materials and Methods

Experimental model and subject details

Six C57BL/6N mice (three male, three female) were housed in a 12-h light/dark cycle in standard ventilated cages under specific pathogen-free conditions with constant temperature (21°C) and humidity (50–60%) and fed ad libitum with a standard mouse diet. At the age of 18–21 wk, mice were euthanized by cervical dislocation. The study was approved by the by the Landesamt für Natur, Umwelt und Verbraucherschutz Nordrhein–Westfalen, Germany, and performed in accordance with European law.

Tissue preparation and isolation of ultrapure mitochondria

Mice were euthanized by cervical dislocation and the seven tissues—heart, SKM, BAT, spleen, kidney, liver, and brain—were rapidly removed. Heart, spleen, and kidney were homogenized in mitochondrial isolation buffer containing 320 mM sucrose, 1 mM EDTA, and 10 mM Tris–HCl, pH 7.4, supplemented with EDTA-free complete protease inhibitor cocktail and PhosSTOP tablets (Roche). For isolation of mitochondria from BAT, liver, and brain, the mitochondrial isolation buffer was additionally supplemented with 0.2% BSA (Sigma-Aldrich). Subsequently, crude mitochondria were isolated from the homogenates by two rounds of differential centrifugation (see Fig 1A). Isolation of crude mitochondria from SKM was performed as previously described (Frezza et al, 2007). Crude mitochondrial pellets from all tissues were further purified on a Percoll density gradient as described recently (Kühl et al, 2017). Briefly, mitochondrial pellets were washed once in 1xM buffer (220 mM mannitol, 70 mM sucrose, 5 mM HEPES pH 7.4, 1 mM EGTA pH 7.4; pH was adjusted with potassium hydroxide; supplemented with EDTA-free complete protease inhibitor cocktail and PhosSTOP tablets [Roche]); and subsequently purified on a Percoll (GE healthcare) density gradient of 12%:19%:40% via centrifugation in a SW41 rotor at 42,000*g* at 4°C for 30 min in a Beckman Coulter Optima L-100 XP ultracentrifuge using 14 × 89 mm Ultra-Clear Centrifuge Tubes (Beckman Instruments Inc.). Ultrapure mitochondria were harvested at the interphase between 19% and 40% and washed three times with 1xM buffer. Dry mitochondrial pellets were snap-frozen in liquid nitrogen and stored at −80°C until further use.

Western blot and antisera

The protein concentration of protein samples was determined using the RCDC assay (Bio-Rad) and BSA as a standard. For standard gel electrophoresis, protein samples (40–60 μg/lane) were mixed with 2x NuPAGE LDS sample buffer supplemented with 200 mM DTT, heated for 10 min, and resolved using commercially available 4–12% NuPAGE Bis–Tris gels and MOPS buffer (Invitrogen) including protein standards (Spectra Multicolor Broad Range; Thermo Fisher Scientific). Proteins were transferred on polyvinylidene difluoride membranes (GE Healthcare) using wet tank blotting (25 mM Tris, 192 mM glycine, and 20% ethanol) at 4°C overnight at 80 mA. Membranes were incubated for 15 min in Ponceau S solution (Sigma-Aldrich) or Coomassie Blue, and blocked in 5% milk-1x TBS-0.1% Tween 20 (TBST) for at least 1 h at RT. Membranes were subsequently incubated with primary antibodies diluted in 3% milk-TBST overnight at 4°C, washed in TBST and incubated with HRP-conjugated secondary antibodies for 2 h at RT. After washing with TBST, immunodetection was performed by enhanced chemiluminescence (Immun-Star HRP Luminol/Enhancer from Bio-Rad) using the ChemiDoc Imaging System (Bio-Rad) and ImageLab software (Bio-Rad). The following antibodies were used to verify purity of different fractions: actin (ab8224; Abcam), histone 3 (Sigma-Aldrich), GADPH (GTX627408; GeneTex), PDI (GTX30716; GeneTex), TFAM (ab131607; Abcam), tubulin (clone 11H10, 2125; Cell Signaling), VDAC1 (clone N152B/23, MABN504; Millipore).

Mitochondrial (phospho)proteome sample preparation

Frozen ultrapure mitochondria pellets were resuspended in lysis buffer (4% SDC, 100 mM Tris/HCl, pH 8.5), boiled for 5 min at 95°C, and sonicated in 30 s intervals for 15 min (Bioruptor). Protein concentration was estimated via Tryptophan assay (Kulak et al, 2014) and was adjusted with lysis buffer to a total volume of 270 μl containing 400 μg of protein for brain, SKM, liver, heart, kidney, and 140 μg of protein for BAT samples. Proteins were reduced and alkylated by adding 30 μl of 10x reduction/alkylation solution 100 mM Tris (2-carboxyethyl)phosphine hydrochloride and 400 mM 2-chloroacetamide, followed by 5 min incubation at 45°C. Subsequently, 1:100 trypsin and LysC were added for overnight protein digestion at 37°C. For proteome analysis, 10 μl (brain, SKM, liver, heart, kidney) and 20 μl (BAT, spleen) aliquots were taken and loaded on SDB-RPS StageTips. Peptides were washed with 200 μl wash buffer (0.2% TFA/2% ACN [vol/vol]) and then eluted with SDB-RPS elution buffer (1.25% NH_4OH, 80% ACN [vol/vol]) and dried in a SpeedVac. Dried peptides were resuspended in A* buffer (2% ACN/0.1% TFA).

The remaining samples were processed following the EasyPhos protocol for phosphopeptide enrichment (Humphrey et al, 2018). In brief, samples were first mixed with isopropanol and EP buffer (48% TFA, 8 mM KH_2PO_4), followed by phosphopeptide enrichment with 5 mg TiO_2 beads per sample (GL Sciences). For this, samples were mixed with TiO_2 beads in loading buffer (6% TFA/80% ACN [vol/vol]) at a concentration of 1 mg/μl and incubated on a ThermoMixer (Eppendorf) for 5 min at 40°C by shaking at 1,200 rpm. Subsequently, beads were washed four times with 1 ml of wash buffer (5% TFA, 60% isopropanol [vol/vol]) and phosphopeptides were eluted from beads using 60 μl of elution buffer (40% ACN, 5% NH_4OH) and concentrated in a SpeedVac for 30 min at 45°C. Samples were immediately diluted with 100 μl of SDBRPS loading buffer (99% isopropanol, 1% TFA [vol/vol]) and loaded on SDB-RPS StageTips.

Thereafter, phosphopeptides were washed and eluted as described above and resuspended in 6 μl A*.

LC-MS/MS

For all measurements, peptides were loaded onto a 50-cm, in-house packed, reversed-phase column (75 μm inner diameter, 1. diameter, ReproSil-Pur C18-AQ 1.9 μm resin [Dr. Maisch GmbH]) and separated with and binary buffer system consisting of buffer A (0.1% formic acid [FA]) and buffer B (0.1% FA in 80% ACN). The column temperature was controlled by a homemade column oven and maintained at 60°C. For nanoflow liquid chromatography, an EASY-nLC 1,200 system (Thermo Fisher Scientific), directly coupled online with a Q Exactive HF-X (Thermo Fisher Scientific) via a nano-electrospray source, was operated at a flow rate of 300 and 350 nl/min for mitochondrial proteome and phosphoproteome measurements, respectively.

For mitochondrial proteome measurements, 500 ng of peptides were loaded and separated using a gradient starting at 5% buffer B, increasing to 30% buffer B in 80 min, 60% buffer B in 4 min and 95% buffer B in 4 min. The MS was operated in DDA mode (Top12) with a full scan range of 300–1,650 m/z and a MS1 and MS2 resolution of 60,000 and 15,000, respectively. The automatic gain control was set to 3×10^6 and 1×10^5 for MS1 and MS2, whereas the maximum injection time was set to 20 and 60 ms, respectively. Precursor ion selection width was kept at 1.4 m/z and fragmentation was achieved by higher-energy collisional dissociation (NCE 27%). Dynamic exclusion was enabled and set to 20 s.

For mitochondrial phosphoproteome measurements, 5 μl as loaded and separated using a gradient starting at 3% buffer B, increasing to 19% buffer B in 40 min, 41% buffer B in 20 min, and 90% buffer B in 5 min. The MS was operated in DDA mode (Top10) with a full scan range of 300–1,600 and a MS1 and MS2 resolution of 60,000 and 15,000, respectively. The automatic gain control was set to 3×10^6 and 1×10^5 for MS1 and MS2, wherea the maximum injection time was set to 120 and 60 ms, respectively. Precursor ion selection width was kept at 1.6 m/z and fragmentation was achieved by higher energy collisional dissociation (NCE 27%). Dynamic exclusion was enabled and set to 30 s.

Raw data analysis

DDA raw data were analyzed with MaxQuant (1.6.14.0) against the mouse fasta file (downloaded 19. October 2020) using default settings. PSM and protein dales discovery rate were controlled at 1% FDR. The match between runs functionality was enabled and set in a way that only biological replicates belonging to the same tissue type were allowed to match each other. This eliminates the possibility of potentially false match between runs identification transfer between tissues. Carbamidomethyl (C) was selected as fixed modification and acetyl (Protein N-term) and oxidation (M) were defined as variable modifications. For mitochondrial phosphoproteome analysis, STY site phosphorylation was additionally selected as variable modification.

Bioinformatics analysis

Data analysis was performed using the python programing language using python (3.8.12) and the following packages: alphamap, matplotlib (3.5.0), mygene (3.2.2), numpy (1.19.2), pandas (1.1.3), pyteomics (4.3.3), requests (2.26.0), scipy (1.7.2), seaborn (0.11.2), sklearn (0.0), upsetplot (0.6.0). All notebooks used for data analysis are available at GitHub (https://github.com/MannLabs). Identified proteins were filtered for at least three valid values in at least one tissue. Similarly, phosphorylation sites were filtered for at least five valid values in at least one tissue and a localization probability >75%. The UniProt API was used to map "ACC + ID" protein group identifiers provided by the MQ analysis to "ENSEMBL_ID," "P_ENTREZGENEID" and "STRING_ID" for further analysis. "ENSEMBL_ID" and "P_ENTREZGENEID" identifier were used for mitochondrial protein annotation based on the IMPI (IMPI_2021_Q4, downloaded 27. October 2020) and MitoCarta3.0 (downloaded 1. January 2021) databases, respectively. Network analysis and visualization were performed with the StringApp (1.6.0) in Cytoscape (3.8.2). Kinase annotations are based on manual annotations (SourceDataForFigure6) and "pkinfam" (downloaded 9. Arpil 2021). Networkin3.0 was used for KSA predictions, whereas the Networkin score was set to 1. Gene Ontology (GO) annotations for the Geno Ontology biological process term enrichment analysis were retrieved from UniProt (accessed 8. March 2021). Enrichment analysis was performed in Perseus (1.6.7.0) against the set of identified proteins in the corresponding tissue and the results were filtered for an intersection size >10. Missing values were only imputed for principle component analysis and heatmap analysis. For this, a Gaussian normal distribution with a width of 0.3 relative to the SD of measured values and a downshift of 1.8 SDs were used. For data normalization, intensity values were $\log_2$ transformed and then filtered for known proteins. The median value of these mitochondrial proteins was subtracted from all $\log_2$ transformed values. Significance testing for individual proteins and phosphopeptides as shown in Figs 3 and 7 was performed with the ordinary one-way ANOVA method or by two-sided *t* tests in GraphPad Prism (9.3.1) (SourceDataForFigure3, SourceDataForFigure7). Significance testing for differences in mitochondrial protein, phosphoprotein, and phosphosite localization was performed in RStudio (1.3.1093) (SourceDataForFigure6). OMM proportions were used for fitting a beta-regression model using the betareg R package with default settings (Cribari-Neto & Zeileis, 2010; Grun et al, 2012). *P*-values were estimated with the lrtest function of the lmtest package (Zeileis & Hothorn, 2015) and *P*-values were adjusted with the "fdr" method of the *P*.adjust function of the stats base package (Benjamini & Hochberg, 1995).

Website tool

The website tool is structured into four sections. The first three "Pathway view," "Sequence view," and "Tissue comparison" are for displaying data, whereas the fourth section provides explanations for each individual section. In the "Pathway view" and "Tissue comparison," proteome and phosphoproteome data filtered for at least three and five identifications in at least one tissue,

respectively. Intensity values were normalized as described above and used for data representation in the "Tissue comparison" tab or z-scored across tissues and used for the "Pathway view tab." Here, median z-score values of the six biological replicates per tissue are displayed in the data table. The polar plot represents the median z-score of all pathway/complex members of a given tissue. Network/complex annotations were retrieved from MitoCarta3.0 and protein interactions are based on STRING interaction scores. These STRING interaction scores were retrieved from STRING (17. November 2021) using the "STRING_ID" and the STRING API. For the "Sequence view," the "evidence.txt" of the MaxQuant output files was directly used as input to annotated sequences.

The python programming language was used for data processing and visualization for the dashboard. The following libraries were used for data processing: numpy (1.19.2), pandas (1.19.2), re, sys, os, and pyteomics (4.3.3). Several libraries from the HoloViz family of tools were used for data visualization and creation of the dashboard, including panel (1.14.6), holoviews (1.14.6), bokeh (2.2.2), plotly (4.12.0), and param (1.10.0). Network visualization was achieved with the NetworkX package (Hagberg et al, 2008). The Alphamap tool (Voytik et al, 2022) was integrated to display linear protein sequence annotations and to visualize 3D protein structures.

Data Availability

Datasets generated in this study have been deposited at ProteomeXchange and are publicly available (Identifier: PXD030062). All original code has been deposited on GitHub (https://github.com/MannLabs) and is available as of the date of publication. Any additional information required to reanalyze the data reported in this article is available from the lead contact upon request.

Supplementary Information

Supplementary Information is available at https://doi.org/10.26508/lsa.202302147.

Acknowledgements

This work was supported by grants to N-G Larsson from the Swedish Research Council (2015-00418), Swedish Cancer Foundation (2021.1409), the Knut and Alice Wallenberg foundation, European Research Council (ERC Advanced Grant 2016-741366), grants from the Swedish state under the agreement between the Swedish government and the county councils (SLL2018.0471). LS Kremer was supported by an EMBO long-term fellowship (ALTF 570-2019). I Kühl was supported by the French Muscular Dystrophy Association (AFM-Téléthon #23294) and Agence nationale de la recherche (ANR-20-CE12-0011). We thank all members of the Department of Signal Transduction and Proteomics, in particular, Isabel Bludau for helpful discussions regarding the website tool, Igor Paron for MS technical assistance, Mario Oroshi for technical assistance during website setup, Marta Murgia for helpful discussions on mitochondrial biology, and Johannes Müller-Reif, Patricia Skowronek, and Sophia Steigerwald for columns. We are grateful to Jesper Olsen, Brenda Schulman, and Maria Miranda for constructive and insightful discussions. Figs 1A and 6A were partly created with BioRender.com.

Author Contributions

FM Hansen: conceptualization, software, formal analysis, investigation, visualization, methodology, and writing—original draft, review, and editing.
LS Kremer: conceptualization, formal analysis, investigation, methodology, and writing—original draft, review, and editing.
O Karayel: conceptualization, formal analysis, methodology, and writing—review and editing.
I Bludau: data curation, software, methodology, and writing—review and editing.
N-G Larsson: conceptualization, resources, supervision, funding acquisition, project administration, and writing—review and editing.
I Kühl: conceptualization, investigation, methodology, and writing—review and editing.
M Mann: conceptualization, supervision, funding acquisition, project administration, and writing—original draft, review, and editing.

Conflict of Interest Statement

The authors declare that they have no conflict of interest.

References

Anderson S, Bankier AT, Barrell BG, de Bruijn MH, Coulson AR, Drouin J, Eperon IC, Nierlich DP, Roe BA, Sanger F, et al (1981) Sequence and organization of the human mitochondrial genome. *Nature* 290: 457–465. doi:10.1038/290457a0

Anunciado-Koza RP, Zhang J, Ukropec J, Bajpeyi S, Koza RA, Rogers RC, Cefalu WT, Mynatt RL, Kozak LP (2011) Inactivation of the mitochondrial carrier SLC25A25 (ATP-Mg2+/Pi transporter) reduces physical endurance and metabolic efficiency in mice. *J Biol Chem* 286: 11659–11671. doi:10.1074/jbc.M110.203000

Aponte AM, Phillips D, Hopper RK, Johnson DT, Harris RA, Blinova K, Boja ES, French S, Balaban RS (2009) Use of (32)P to study dynamics of the mitochondrial phosphoproteome. *J Proteome Res* 8: 2679–2695. doi:10.1021/pr800913j

Baines CP, Zhang J, Wang GW, Zheng YT, Xiu JX, Cardwell EM, Bolli R, Ping P (2002) Mitochondrial PKCepsilon and MAPK form signaling modules in the murine heart: Enhanced mitochondrial PKCepsilon-MAPK interactions and differential MAPK activation in PKCepsilon-induced cardioprotection. *Circ Res* 90: 390–397. doi:10.1161/01.res.0000012702.90501.8d

Bak S, León IR, Jensen ON, Højlund K (2013) Tissue specific phosphorylation of mitochondrial proteins isolated from rat liver, heart muscle, and skeletal muscle. *J Proteome Res* 12: 4327–4339. doi:10.1021/pr400281r

Basch M, Wagner M, Rolland S, Carbonell A, Zeng R, Khosravi S, Schmidt A, Aftab W, Imhof A, Wagener J, et al (2020) Msp1 cooperates with the proteasome for extraction of arrested mitochondrial import intermediates. *Mol Biol Cell* 31: 753–767. doi:10.1091/mbc.E19-06-0329

Bayraktar EC, Baudrier L, Ozerdem C, Lewis CA, Chan SH, Kunchok T, Abu-Remaileh M, Cangelosi AL, Sabatini DM, Birsoy K, et al (2019) MITO-tag mice enable rapid isolation and multimodal profiling of mitochondria from specific cell types in vivo. *Proc Natl Acad Sci U S A* 116: 303–312. doi:10.1073/pnas.1816656115

Becker Y, Loignon RC, Julien AS, Marcoux G, Allaeys I, Lévesque T, Rollet-Labelle E, Benk-Fortin H, Cloutier N, Melki I, et al (2019) Anti-mitochondrial autoantibodies in systemic lupus erythematosus and their association with disease manifestations. *Sci Rep* 9: 4530. doi:10.1038/s41598-019-40900-3

Bekker-Jensen DB, Bernhardt OM, Hogrebe A, Martinez-Val A, Verbeke L, Gandhi T, Kelstrup CD, Reiter L, Olsen JV (2020) Rapid and site-specific deep phosphoproteome profiling by data-independent acquisition without the need for spectral libraries. *Nat Commun* 11: 787. doi:10.1038/s41467-020-14609-1

Ben-Menachem R, Tal M, Shadur T, Pines O (2011) A third of the yeast mitochondrial proteome is dual localized: A question of evolution. *Proteomics* 11: 4468–4476. doi:10.1002/pmic.201100199

Benincá C, Planagumà J, de Freitas Shuck A, Acín-Perez R, Muñoz JP, de Almeida MM, Brown JH, Murphy AN, Zorzano A, Enríquez JA, et al (2014) A new non-canonical pathway of Gα(q) protein regulating mitochondrial dynamics and bioenergetics. *Cell Signal* 26: 1135–1146. doi:10.1016/j.cellsig.2014.01.009

Benjamini Y, Hochberg Y (1995) Controlling the false discovery rate: A practical and powerful approach to multiple testing. *J R Stat Soc Ser B* 57: 289–300. doi:10.1111/j.2517-6161.1995.tb02031.x

Bleazard W, McCaffery JM, King EJ, Bale S, Mozdy A, Tieu Q, Nunnari J, Shaw JM (1999) The dynamin-related GTPase Dnm1 regulates mitochondrial fission in yeast. *Nat Cell Biol* 1: 298–304. doi:10.1038/13014

Bock FJ, Tait SWG (2020) Mitochondria as multifaceted regulators of cell death. *Nat Rev Mol Cell Biol* 21: 85–100. doi:10.1038/s41580-019-0173-8

Bohnert M, Zerbes RM, Davies KM, Mühleip AW, Rampelt H, Horvath SE, Boenke T, Kram A, Perschil I, Veenhuis M, et al (2015) Central role of Mic10 in the mitochondrial contact site and cristae organizing system. *Cell Metab* 21: 747–755. doi:10.1016/j.cmet.2015.04.007

Boja ES, Phillips D, French SA, Harris RA, Balaban RS (2009) Quantitative mitochondrial phosphoproteomics using iTRAQ on an LTQ-orbitrap with high energy collision dissociation. *J Proteome Res* 8: 4665–4675. doi:10.1021/pr900387b

Calvo SE, Mootha VK (2010) The mitochondrial proteome and human disease. *Annu Rev Genomics Hum Genet* 11: 25–44. doi:10.1146/annurev-genom-082509-141720

Cereghetti GM, Stangherlin A, Martins de Brito O, Chang CR, Blackstone C, Bernardi P, Scorrano L (2008) Dephosphorylation by calcineurin regulates translocation of Drp1 to mitochondria. *Proc Natl Acad Sci U S A* 105: 15803–15808. doi:10.1073/pnas.0808249105

Cioni JM, Lin JQ, Holtermann AV, Koppers M, Jakobs MAH, Azizi A, Turner-Bridger B, Shigeoka T, Franze K, Harris WA, et al (2019) Late endosomes act as mRNA translation platforms and sustain mitochondria in axons. *Cell* 176: 56–72.e15. doi:10.1016/j.cell.2018.11.030

Colina-Tenorio L, Horten P, Pfanner N, Rampelt H (2020) Shaping the mitochondrial inner membrane in health and disease. *J Intern Med* 287: 645–664. doi:10.1111/joim.13031

Cribari-Neto F, Zeileis A (2010) Beta regression in R. *J Stat Softw* 34: 1–24. doi:10.18637/jss.v034.i02

Cribbs JT, Strack S (2007) Reversible phosphorylation of Drp1 by cyclic AMP-dependent protein kinase and calcineurin regulates mitochondrial fission and cell death. *EMBO Rep* 8: 939–944. doi:10.1038/sj.embor.7401062

Cui Z, Hou J, Chen X, Li J, Xie Z, Xue P, Cai T, Wu P, Xu T, Yang F (2010) The profile of mitochondrial proteins and their phosphorylation signaling network in INS-1 beta cells. *J Proteome Res* 9: 2898–2908. doi:10.1021/pr100139z

del Arco A, Satrústegui J (2004) Identification of a novel human subfamily of mitochondrial carriers with calcium-binding domains. *J Biol Chem* 279: 24701–24713. doi:10.1074/jbc.M401417200

Deng WJ, Nie S, Dai J, Wu JR, Zeng R (2010) Proteome, phosphoproteome, and hydroxyproteome of liver mitochondria in diabetic rats at early pathogenic stages. *Mol Cell Proteomics* 9: 100–116. doi:10.1074/mcp.M900020-MCP200

Deng N, Zhang J, Zong C, Wang Y, Lu H, Yang P, Wang W, Young GW, Wang Y, Korge P, et al (2011) Phosphoproteome analysis reveals regulatory sites in major pathways of cardiac mitochondria. *Mol Cell Proteomics* 10: M110.000117. doi:10.1074/mcp.M110.000117

Desai R, East DA, Hardy L, Faccenda D, Rigon M, Crosby J, Alvarez MS, Singh A, Mainenti M, Hussey LK, et al (2020) Mitochondria form contact sites with the nucleus to couple prosurvival retrograde response. *Sci Adv* 6: eabc9955. doi:10.1126/sciadv.abc9955

Dikov D, Reichert AS (2011) How to split up: Lessons from mitochondria. *EMBO J* 30: 2751–2753. doi:10.1038/emboj.2011.219

Ducommun S, Deak M, Sumpton D, Ford RJ, Núñez Galindo A, Kussmann M, Viollet B, Steinberg GR, Foretz M, Dayon L, et al (2015) Motif affinity and mass spectrometry proteomic approach for the discovery of cellular AMPK targets: Identification of mitochondrial fission factor as a new AMPK substrate. *Cell Signal* 27: 978–988. doi:10.1016/j.cellsig.2015.02.008

Fecher C, Trovò L, Müller SA, Snaidero N, Wettmarshausen J, Heink S, Ortiz O, Wagner I, Kühn R, Hartmann J, et al (2019) Cell-type-specific profiling of brain mitochondria reveals functional and molecular diversity. *Nat Neurosci* 22: 1731–1742. doi:10.1038/s41593-019-0479-z

Feng J, Zhu M, Schaub MC, Gehrig P, Roschitzki B, Lucchinetti E, Zaugg M (2008) Phosphoproteome analysis of isoflurane-protected heart mitochondria: Phosphorylation of adenine nucleotide translocator-1 on Tyr194 regulates mitochondrial function. *Cardiovasc Res* 80: 20–29. doi:10.1093/cvr/cvn161

Ferreira R, Vitorino R, Alves RM, Appell HJ, Powers SK, Duarte JA, Amado F (2010) Subsarcolemmal and intermyofibrillar mitochondria proteome differences disclose functional specializations in skeletal muscle. *Proteomics* 10: 3142–3154. doi:10.1002/pmic.201000173

Fiermonte G, De Leonardis F, Todisco S, Palmieri L, Lasorsa FM, Palmieri F (2004) Identification of the mitochondrial ATP-Mg/Pi transporter. Bacterial expression, reconstitution, functional characterization, and tissue distribution. *J Biol Chem* 279: 30722–30730. doi:10.1074/jbc.M400445200

Forner F, Foster LJ, Campanaro S, Valle G, Mann M (2006) Quantitative proteomic comparison of rat mitochondria from muscle, heart, and liver. *Mol Cell Proteomics* 5: 608–619. doi:10.1074/mcp.M500298-MCP200

Frezza C, Cipolat S, Scorrano L (2007) Organelle isolation: Functional mitochondria from mouse liver, muscle and cultured fibroblasts. *Nat Protoc* 2: 287–295. doi:10.1038/nprot.2006.478

Gao C, Xu Y, Liang Z, Wang Y, Shang Q, Zhang S, Wang C, Ni M, Wu D, Huang Z, et al (2021) A novel PGAM5 inhibitor LFHP-1c protects blood-brain barrier integrity in ischemic stroke. *Acta Pharm Sin B* 11: 1867–1884. doi:10.1016/j.apsb.2021.01.008

Grimsrud PA, Carson JJ, Hebert AS, Hubler SL, Niemi NM, Bailey DJ, Jochem A, Stapleton DS, Keller MP, Westphall MS, et al (2012) A quantitative map of the liver mitochondrial phosphoproteome reveals posttranslational control of ketogenesis. *Cell Metab* 16: 672–683. doi:10.1016/j.cmet.2012.10.004

Grun B, Kosmidis I, Zeileis A (2012) Extended beta regression in R: Shaken, stirred, mixed, and partitioned. *J Stat Softw* 48: 1–25. doi:10.18637/jss.v048.i11

Guedouari H, Savoie MC, Jean S, Djeungoue-Petga MA, Pichaud N, Hebert-Chatelain E (2020) Multi-omics reveal that c-src modulates the mitochondrial phosphotyrosine proteome and metabolism according to nutrient availability. *Cell Physiol Biochem* 54: 517–537. doi:10.33594/000000237

Hagberg A, Swart P, S Chult D (2008) *Exploring Network Structure, Dynamics, and Function Using NetworkX*. Los Alamos, NM: Los Alamos National Lab.(LANL).

Han Q, Cai T, Tagle DA, Li J (2010) Structure, expression, and function of kynurenine aminotransferases in human and rodent brains. *Cell Mol Life Sci* 67: 353–368. doi:10.1007/s00018-009-0166-4

Hebert-Chatelain E, Desprez T, Serrat R, Bellocchio L, Soria-Gomez E, Busquets-Garcia A, Pagano Zottola AC, Delamarre A, Cannich A, Vincent P, et al (2016) A cannabinoid link between mitochondria and memory. *Nature* 539: 555–559. doi:10.1038/nature20127

Helfenberger KE, Villalba NM, Buchholz B, Boveris A, Poderoso JJ, Gelpi RJ, Poderoso C (2018) Subcellular distribution of ERK phosphorylation in tyrosine and threonine depends on redox status in murine lung cells. *PLoS One* 13: e0193022. doi:10.1371/journal.pone.0193022

Hitosugi T, Fan J, Chung TW, Lythgoe K, Wang X, Xie J, Ge Q, Gu TL, Polakiewicz RD, Roesel JL, et al (2011) Tyrosine phosphorylation of mitochondrial pyruvate dehydrogenase kinase 1 is important for cancer metabolism. *Mol Cell* 44: 864–877. doi:10.1016/j.molcel.2011.10.015

Hopper RK, Carroll S, Aponte AM, Johnson DT, French S, Shen RF, Witzmann FA, Harris RA, Balaban RS (2006) Mitochondrial matrix phosphoproteome: Effect of extra mitochondrial calcium. *Biochemistry* 45: 2524–2536. doi:10.1021/bi052475e

Horn H, Schoof EM, Kim J, Robin X, Miller ML, Diella F, Palma A, Cesareni G, Jensen LJ, Linding R (2014) KinomeXplorer: An integrated platform for kinome biology studies. *Nat Methods* 11: 603–604. doi:10.1038/nmeth.2968

Hornbeck PV, Kornhauser JM, Tkachev S, Zhang B, Skrzypek E, Murray B, Latham V, Sullivan M (2012) PhosphoSitePlus: A comprehensive resource for investigating the structure and function of experimentally determined post-translational modifications in man and mouse. *Nucleic Acids Res* 40: D261–D270. doi:10.1093/nar/gkr1122

Huang B, Gudi R, Wu P, Harris RA, Hamilton J, Popov KM (1998) Isoenzymes of pyruvate dehydrogenase phosphatase. DNA-derived amino acid sequences, expression, and regulation. *J Biol Chem* 273: 17680–17688. doi:10.1074/jbc.273.28.17680

Huang B, Wu P, Popov KM, Harris RA (2003) Starvation and diabetes reduce the amount of pyruvate dehydrogenase phosphatase in rat heart and kidney. *Diabetes* 52: 1371–1376. doi:10.2337/diabetes.52.6.1371

Humphrey SJ, Karayel O, James DE, Mann M (2018) High-throughput and high-sensitivity phosphoproteomics with the EasyPhos platform. *Nat Protoc* 13: 1897–1916. doi:10.1038/s41596-018-0014-9

Hüttemann M, Lee I, Samavati L, Yu H, Doan JW (2007) Regulation of mitochondrial oxidative phosphorylation through cell signaling. *Biochim Biophys Acta* 1773: 1701–1720. doi:10.1016/j.bbamcr.2007.10.001

Jaburek M, Costa AD, Burton JR, Costa CL, Garlid KD (2006) Mitochondrial PKC epsilon and mitochondrial ATP-sensitive K+ channel copurify and coreconstitute to form a functioning signaling module in proteoliposomes. *Circ Res* 99: 878–883. doi:10.1161/01.RES.0000245106.80628.d3

Jadiya P, Tomar D (2020) Mitochondrial protein quality control mechanisms. *Genes (Basel)* 11: 563. doi:10.3390/genes11050563

Jastroch M, Divakaruni AS, Mookerjee S, Treberg JR, Brand MD (2010) Mitochondrial proton and electron leaks. *Essays Biochem* 47: 53–67. doi:10.1042/bse0470053

Johnson DT, Harris RA, French S, Blair PV, You J, Bemis KG, Wang M, Balaban RS (2007) Tissue heterogeneity of the mammalian mitochondrial proteome. *Am J Physiol Cell Physiol* 292: C689–C697. doi:10.1152/ajpcell.00108.2006

Jourdain AA, Popow J, de la Fuente MA, Martinou JC, Anderson P, Simarro M (2017) The FASTK family of proteins: Emerging regulators of mitochondrial RNA biology. *Nucleic Acids Res* 45: 10941–10947. doi:10.1093/nar/gkx772

Jumper J, Evans R, Pritzel A, Green T, Figurnov M, Ronneberger O, Tunyasuvunakool K, Bates R, Žídek A, Potapenko A, et al (2021) Highly accurate protein structure prediction with AlphaFold. *Nature* 596: 583–589. doi:10.1038/s41586-021-03819-2

Kajimura S, Saito M (2014) A new era in brown adipose tissue biology: Molecular control of brown fat development and energy homeostasis. *Annu Rev Physiol* 76: 225–249. doi:10.1146/annurev-physiol-021113-170252

Kappler L, Li J, Häring HU, Weigert C, Lehmann R, Xu G, Hoene M (2016) Purity matters: A workflow for the valid high-resolution lipid profiling of mitochondria from cell culture samples. *Sci Rep* 6: 21107. doi:10.1038/srep21107

Karpova T, Danchuk S, Kolobova E, Popov KM (2003) Characterization of the isozymes of pyruvate dehydrogenase phosphatase: Implications for the regulation of pyruvate dehydrogenase activity. *Biochim Biophys Acta* 1652: 126–135. doi:10.1016/j.bbapap.2003.08.010

Kashatus JA, Nascimento A, Myers LJ, Sher A, Byrne FL, Hoehn KL, Counter CM, Kashatus DF (2015) Erk2 phosphorylation of Drp1 promotes mitochondrial fission and MAPK-driven tumor growth. *Mol Cell* 57: 537–551. doi:10.1016/j.molcel.2015.01.002

Khosravi S, Harner ME (2020) The MICOS complex, a structural element of mitochondria with versatile functions. *Biol Chem* 401: 765–778. doi:10.1515/hsz-2020-0103

Klyuyeva A, Tuganova A, Kedishvili N, Popov KM (2019) Tissue-specific kinase expression and activity regulate flux through the pyruvate dehydrogenase complex. *J Biol Chem* 294: 838–851. doi:10.1074/jbc.RA118.006433

Kodron A, Mussulini BH, Pilecka I, Chacinska A (2021) The ubiquitin-proteasome system and its crosstalk with mitochondria as therapeutic targets in medicine. *Pharmacol Res* 163: 105248. doi:10.1016/j.phrs.2020.105248

Kolitsida P, Zhou J, Rackiewicz M, Nolic V, Dengjel J, Abeliovich H (2019) Phosphorylation of mitochondrial matrix proteins regulates their selective mitophagic degradation. *Proc Natl Acad Sci U S A* 116: 20517–20527. doi:10.1073/pnas.1901759116

Korotchkina LG, Patel MS (2001) Site specificity of four pyruvate dehydrogenase kinase isoenzymes toward the three phosphorylation sites of human pyruvate dehydrogenase. *J Biol Chem* 276: 37223–37229. doi:10.1074/jbc.M103069200

Kotrasová V, Keresztesová B, Ondrovičová G, Bauer JA, Havalová H, Pevala V, Kutejová E, Kunová N (2021) Mitochondrial kinases and the role of mitochondrial protein phosphorylation in health and disease. *Life (Basel)* 11: 82. doi:10.3390/life11020082

Kruse R, Højlund K (2017) Mitochondrial phosphoproteomics of mammalian tissues. *Mitochondrion* 33: 45–57. doi:10.1016/j.mito.2016.08.004

Kühl I, Miranda M, Atanassov I, Kuznetsova I, Hinze Y, Mourier A, Filipovska A, Larsson NG (2017) Transcriptomic and proteomic landscape of mitochondrial dysfunction reveals secondary coenzyme Q deficiency in mammals. *Elife* 6: e30952. doi:10.7554/eLife.30952

Kulak NA, Pichler G, Paron I, Nagaraj N, Mann M (2014) Minimal, encapsulated proteomic-sample processing applied to copy-number estimation in eukaryotic cells. *Nat Methods* 11: 319–324. doi:10.1038/nmeth.2834

Kunji ERS, King MS, Ruprecht JJ, Thangaratnarajah C (2020) The SLC25 carrier family: Important transport proteins in mitochondrial physiology and pathology. *Physiology (Bethesda)* 35: 302–327. doi:10.1152/physiol.00009.2020

Kuznetsov AV, Hermann M, Saks V, Hengster P, Margreiter R (2009) The cell-type specificity of mitochondrial dynamics. *Int J Biochem Cell Biol* 41: 1928–1939. doi:10.1016/j.biocel.2009.03.007

Kwak C, Shin S, Park JS, Jung M, Nhung TTM, Kang MG, Lee C, Kwon TH, Park SK, Mun JY, et al (2020) Contact-ID, a tool for profiling organelle contact sites, reveals regulatory proteins of mitochondrial-associated

membrane formation. *Proc Natl Acad Sci U S A* 117: 12109–12120. doi:10.1073/pnas.1916584117

Lashkevich KA, Dmitriev SE (2021) mRNA targeting, transport and local translation in eukaryotic cells: From the classical view to a diversity of new concepts. *Mol Biol* 55: 507–537. doi:10.1134/S0026893321030080

Lee J, Xu Y, Chen Y, Sprung R, Kim SC, Xie S, Zhao Y (2007) Mitochondrial phosphoproteome revealed by an improved IMAC method and MS/MS/MS. *Mol Cell Proteomics* 6: 669–676. doi:10.1074/mcp.M600218-MCP200

Lewandrowski U, Sickmann A, Cesaro L, Brunati AM, Toninello A, Salvi M (2008) Identification of new tyrosine phosphorylated proteins in rat brain mitochondria. *FEBS Lett* 582: 1104–1110. doi:10.1016/j.febslet.2008.02.077

Lewis TL Jr., Kwon SK, Lee A, Shaw R, Polleux F (2018) MFF-dependent mitochondrial fission regulates presynaptic release and axon branching by limiting axonal mitochondria size. *Nat Commun* 9: 5008. doi:10.1038/s41467-018-07416-2

Lewis SM, Williams A, Eisenbarth SC (2019) Structure and function of the immune system in the spleen. *Sci Immunol* 4: eaau6085. doi:10.1126/sciimmunol.aau6085

Li N, Qian S, Li B, Zhan X (2019) Quantitative analysis of the human ovarian carcinoma mitochondrial phosphoproteome. *Aging (Albany NY)* 11: 6449–6468. doi:10.18632/aging.102199

Liang MZ, Ke TL, Chen L (2021) Mitochondrial protein PGAM5 emerges as a new regulator in neurological diseases. *Front Mol Neurosci* 14: 730604. doi:10.3389/fnmol.2021.730604

Liesa M, Palacín M, Zorzano A (2009) Mitochondrial dynamics in mammalian health and disease. *Physiol Rev* 89: 799–845. doi:10.1152/physrev.00030.2008

Liu T, Yu R, Jin SB, Han L, Lendahl U, Zhao J, Nistér M (2013) The mitochondrial elongation factors MIEF1 and MIEF2 exert partially distinct functions in mitochondrial dynamics. *Exp Cell Res* 319: 2893–2904. doi:10.1016/j.yexcr.2013.07.010

Liu YJ, McIntyre RL, Janssens GE, Houtkooper RH (2020) Mitochondrial fission and fusion: A dynamic role in aging and potential target for age-related disease. *Mech Ageing Dev* 186: 111212. doi:10.1016/j.mad.2020.111212

Losón OC, Song Z, Chen H, Chan DC (2013) Fis1, Mff, MiD49, and MiD51 mediate Drp1 recruitment in mitochondrial fission. *Mol Biol Cell* 24: 659–667. doi:10.1091/mbc.E12-10-0721

Lu W, Karuppagounder SS, Springer DA, Allen MD, Zheng L, Chao B, Zhang Y, Dawson VL, Dawson TM, Lenardo M (2014) Genetic deficiency of the mitochondrial protein PGAM5 causes a Parkinson's-like movement disorder. *Nat Commun* 5: 4930. doi:10.1038/ncomms5930

Lu X, Gong Y, Hu W, Mao Y, Wang T, Sun Z, Su X, Fu G, Wang Y, Lai D (2022) Ultrastructural and proteomic profiling of mitochondria-associated endoplasmic reticulum membranes reveal aging signatures in striated muscle. *Cell Death Dis* 13: 296. doi:10.1038/s41419-022-04746-4

Majumder PK, Pandey P, Sun X, Cheng K, Datta R, Saxena S, Kharbanda S, Kufe D (2000) Mitochondrial translocation of protein kinase C delta in phorbol ester-induced cytochrome c release and apoptosis. *J Biol Chem* 275: 21793–21796. doi:10.1074/jbc.C000048200

Malherbe P, Alberati-Giani D, Köhler C, Cesura AM (1995) Identification of a mitochondrial form of kynurenine aminotransferase/glutamine transaminase K from rat brain. *FEBS Lett* 367: 141–144. doi:10.1016/0014-5793(95)00546-l

McBride HM, Neuspiel M, Wasiak S (2006) Mitochondria: More than just a powerhouse. *Curr Biol* 16: R551–R560. doi:10.1016/j.cub.2006.06.054

McLaughlin KL, Hagen JT, Coalson HS, Nelson MAM, Kew KA, Wooten AR, Fisher-Wellman KH (2020) Novel approach to quantify mitochondrial content and intrinsic bioenergetic efficiency across organs. *Sci Rep* 10: 17599. doi:10.1038/s41598-020-74718-1

Menacho C, Prigione A (2020) Tackling mitochondrial diversity in brain function: From animal models to human brain organoids. *Int J Biochem Cell Biol* 123: 105760. doi:10.1016/j.biocel.2020.105760

Montes de Oca Balderas P (2021) Mitochondria-plasma membrane interactions and communication. *J Biol Chem* 297: 101164. doi:10.1016/j.jbc.2021.101164

Moore AS, Holzbaur ELF (2018) Mitochondrial-cytoskeletal interactions: Dynamic associations that facilitate network function and remodeling. *Curr Opin Physiol* 3: 94–100. doi:10.1016/j.cophys.2018.03.003

Mootha VK, Bunkenborg J, Olsen JV, Hjerrild M, Wisniewski JR, Stahl E, Bolouri MS, Ray HN, Sihag S, Kamal M, et al (2003) Integrated analysis of protein composition, tissue diversity, and gene regulation in mouse mitochondria. *Cell* 115: 629–640. doi:10.1016/s0092-8674(03)00926-7

Morgenstern M, Peikert CD, Lübbert P, Suppanz I, Klemm C, Alka O, Steiert C, Naumenko N, Schendzielorz A, Melchionda L, et al (2021) Quantitative high-confidence human mitochondrial proteome and its dynamics in cellular context. *Cell Metab* 33: 2464–2483.e18. doi:10.1016/j.cmet.2021.11.001

Niemi NM, Pagliarini DJ (2021) The extensive and functionally uncharacterized mitochondrial phosphoproteome. *J Biol Chem* 297: 100880. doi:10.1016/j.jbc.2021.100880

Niemi NM, Wilson GM, Overmyer KA, Vögtle FN, Myketin L, Lohman DC, Schueler KL, Attie AD, Meisinger C, Coon JJ, et al (2019) Pptc7 is an essential phosphatase for promoting mammalian mitochondrial metabolism and biogenesis. *Nat Commun* 10: 3197. doi:10.1038/s41467-019-11047-6

Nunnari J, Suomalainen A (2012) Mitochondria: In sickness and in health. *Cell* 148: 1145–1159. doi:10.1016/j.cell.2012.02.035

Oelkrug R, Polymeropoulos ET, Jastroch M (2015) Brown adipose tissue: Physiological function and evolutionary significance. *J Comp Physiol B* 185: 587–606. doi:10.1007/s00360-015-0907-7

Ogbi M, Johnson JA (2006) Protein kinase Cepsilon interacts with cytochrome c oxidase subunit IV and enhances cytochrome c oxidase activity in neonatal cardiac myocyte preconditioning. *Biochem J* 393: 191–199. doi:10.1042/BJ20050757

Pagliarini DJ, Calvo SE, Chang B, Sheth SA, Vafai SB, Ong SE, Walford GA, Sugiana C, Boneh A, Chen WK, et al (2008) A mitochondrial protein compendium elucidates complex I disease biology. *Cell* 134: 112–123. doi:10.1016/j.cell.2008.06.016

Palmieri F, Monné M (2016) Discoveries, metabolic roles and diseases of mitochondrial carriers: A review. *Biochim Biophys Acta* 1863: 2362–2378. doi:10.1016/j.bbamcr.2016.03.007

Panda S, Srivastava S, Li Z, Vaeth M, Fuhs SR, Hunter T, Skolnik EY (2016) Identification of PGAM5 as a mammalian protein histidine phosphatase that plays a central role to negatively regulate CD4(+) T cells. *Mol Cell* 63: 457–469. doi:10.1016/j.molcel.2016.06.021

Patel MS, Nemeria NS, Furey W, Jordan F (2014) The pyruvate dehydrogenase complexes: Structure-based function and regulation. *J Biol Chem* 289: 16615–16623. doi:10.1074/jbc.R114.563148

Perrone M, Caroccia N, Genovese I, Missiroli S, Modesti L, Pedriali G, Vezzani B, Vitto VAM, Antenori M, Lebiedzinska-Arciszewska M, et al (2020) The role of mitochondria-associated membranes in cellular homeostasis and diseases. *Int Rev Cell Mol Biol* 350: 119–196. doi:10.1016/bs.ircmb.2019.11.002

Ping P, Song C, Zhang J, Guo Y, Cao X, Li RC, Wu W, Vondriska TM, Pass JM, Tang XL, et al (2002) Formation of protein kinase C(epsilon)-Lck signaling modules confers cardioprotection. *J Clin Invest* 109: 499–507. doi:10.1172/JCI13200

Rangaraju V, Lauterbach M, Schuman EM (2019) Spatially stable mitochondrial compartments fuel local translation during plasticity. *Cell* 176: 73–84.e15. doi:10.1016/j.cell.2018.12.013

Rath S, Sharma R, Gupta R, Ast T, Chan C, Durham TJ, Goodman RP, Grabarek Z, Haas ME, Hung WHW, et al (2021) MitoCarta3.0: An updated

mitochondrial proteome now with sub-organelle localization and pathway annotations. *Nucleic Acids Res* 49: D1541–D1547. doi:10.1093/nar/gkaa1011

Roberts RF, Bayne AN, Goiran T, Lévesque D, Boisvert FM, Trempe JF, Fon EA (2021) Proteomic profiling of mitochondrial-derived vesicles in brain reveals enrichment of respiratory complex sub-assemblies and small TIM chaperones. *J Proteome Res* 20: 506–517. doi:10.1021/acs.jproteome.0c00506

Rochette L, Meloux A, Zeller M, Malka G, Cottin Y, Vergely C (2020) Mitochondrial SLC25 carriers: Novel targets for cancer therapy. *Molecules* 25: 2417. doi:10.3390/molecules25102417

Rosenberger FA, Atanassov I, Moore D, Calvo-Garrido J, Moedas MF, Wedell A, Freyer C, Wredenberg A (2021) Stable isotope labeling of amino acids in flies (SILAF) reveals differential phosphorylation of mitochondrial proteins upon loss of OXPHOS subunits. *Mol Cell Proteomics* 20: 100065. doi:10.1016/j.mcpro.2021.100065

Rueda CB, Traba J, Amigo I, Llorente-Folch I, González-Sánchez P, Pardo B, Esteban JA, del Arco A, Satrústegui J (2015) Mitochondrial ATP-Mg/Pi carrier SCaMC-3/Slc25a23 counteracts PARP-1-dependent fall in mitochondrial ATP caused by excitotoxic insults in neurons. *J Neurosci* 35: 3566–3581. doi:10.1523/JNEUROSCI.2702-14.2015

Ruprecht JJ, Kunji ERS (2020) The SLC25 mitochondrial carrier family: Structure and mechanism. *Trends Biochem Sci* 45: 244–258. doi:10.1016/j.tibs.2019.11.001

Russell OM, Gorman GS, Lightowlers RN, Turnbull DM (2020) Mitochondrial diseases: Hope for the future. *Cell* 181: 168–188. doi:10.1016/j.cell.2020.02.051

Sadana P, Geyer R, Pezoldt J, Helmsing S, Huehn J, Hust M, Dersch P, Scrima A (2018) The invasin D protein from Yersinia pseudotuberculosis selectively binds the Fab region of host antibodies and affects colonization of the intestine. *J Biol Chem* 293: 8672–8690. doi:10.1074/jbc.RA117.001068

Sandhu SK, Fassan M, Volinia S, Lovat F, Balatti V, Pekarsky Y, Croce CM (2013) B-cell malignancies in microRNA Eμ-miR-17~92 transgenic mice. *Proc Natl Acad Sci U S A* 110: 18208–18213. doi:10.1073/pnas.1315365110

Sathe G, Deepha S, Gayathri N, Nagappa M, Parayil Sankaran B, Taly AB, Khanna T, Pandey A, Govindaraj P (2021) Ethylmalonic encephalopathy ETHE1 p. D165H mutation alters the mitochondrial function in human skeletal muscle proteome. *Mitochondrion* 58: 64–71. doi:10.1016/j.mito.2021.02.011

Schulenberg B, Aggeler R, Beechem JM, Capaldi RA, Patton WF (2003) Analysis of steady-state protein phosphorylation in mitochondria using a novel fluorescent phosphosensor dye. *J Biol Chem* 278: 27251–27255. doi:10.1074/jbc.C300189200

Shai N, Yifrach E, van Roermund CWT, Cohen N, Bibi C, IJlst L, Cavellini L, Meurisse J, Schuster R, Zada L, et al (2018) Systematic mapping of contact sites reveals tethers and a function for the peroxisome-mitochondria contact. *Nat Commun* 9: 1761. doi:10.1038/s41467-018-03957-8

Silva Ramos E, Motori E, Brüser C, Kühl I, Yeroslaviz A, Ruzzenente B, Kauppila JHK, Busch JD, Hultenby K, Habermann BH, et al (2019) Mitochondrial fusion is required for regulation of mitochondrial DNA replication. *PLoS Genet* 15: e1008085. doi:10.1371/journal.pgen.1008085

Smith AC, Robinson AJ (2019) MitoMiner v4.0: An updated database of mitochondrial localization evidence, phenotypes and diseases. *Nucleic Acids Res* 47: D1225–D1228. doi:10.1093/nar/gky1072

Spinelli JB, Haigis MC (2018) The multifaceted contributions of mitochondria to cellular metabolism. *Nat Cell Biol* 20: 745–754. doi:10.1038/s41556-018-0124-1

Stefely JA, Licitra F, Laredj L, Reidenbach AG, Kemmerer ZA, Grangeray A, Jaeg-Ehret T, Minogue CE, Ulbrich A, Hutchins PD, et al (2016) Cerebellar ataxia and coenzyme Q deficiency through loss of unorthodox kinase activity. *Mol Cell* 63: 608–620. doi:10.1016/j.molcel.2016.06.030

Suomalainen A, Battersby BJ (2018) Mitochondrial diseases: The contribution of organelle stress responses to pathology. *Nat Rev Mol Cell Biol* 19: 77–92. doi:10.1038/nrm.2017.66

Taguchi N, Ishihara N, Jofuku A, Oka T, Mihara K (2007) Mitotic phosphorylation of dynamin-related GTPase Drp1 participates in mitochondrial fission. *J Biol Chem* 282: 11521–11529. doi:10.1074/jbc.M607279200

Toyama EQ, Herzig S, Courchet J, Lewis TL Jr., Losón OC, Hellberg K, Young NP, Chen H, Polleux F, Chan DC, et al (2016) Metabolism. AMP-activated protein kinase mediates mitochondrial fission in response to energy stress. *Science* 351: 275–281. doi:10.1126/science.aab4138

Traba J, Del Arco A, Duchen MR, Szabadkai G, Satrústegui J (2012) SCaMC-1 promotes cancer cell survival by desensitizing mitochondrial permeability transition via ATP/ADP-mediated matrix Ca(2+) buffering. *Cell Death Differ* 19: 650–660. doi:10.1038/cdd.2011.139

van der Bliek AM, Shen Q, Kawajiri S (2013) Mechanisms of mitochondrial fission and fusion. *Cold Spring Harb Perspect Biol* 5: a011072. doi:10.1101/cshperspect.a011072

Ventura-Clapier R, Garnier A, Veksler V, Joubert F (2011) Bioenergetics of the failing heart. *Biochim Biophys Acta* 1813: 1360–1372. doi:10.1016/j.bbamcr.2010.09.006

Volkert MR, Crowley DJ (2020) Preventing neurodegeneration by controlling oxidative stress: The role of OXR1. *Front Neurosci* 14: 611904. doi:10.3389/fnins.2020.611904

Voytik E, Bludau I, Willems S, Hansen FM, Brunner AD, Strauss MT, Mann M (2022) AlphaMap: An open-source python package for the visual annotation of proteomics data with sequence specific knowledge. *Bioinformatics* 38: 849–852. doi:10.1093/bioinformatics/btab674

Watanabe T, Saotome M, Nobuhara M, Sakamoto A, Urushida T, Katoh H, Satoh H, Funaki M, Hayashi H (2014) Roles of mitochondrial fragmentation and reactive oxygen species in mitochondrial dysfunction and myocardial insulin resistance. *Exp Cell Res* 323: 314–325. doi:10.1016/j.yexcr.2014.02.027

Wieckowski MR, Giorgi C, Lebiedzinska M, Duszynski J, Pinton P (2009) Isolation of mitochondria-associated membranes and mitochondria from animal tissues and cells. *Nat Protoc* 4: 1582–1590. doi:10.1038/nprot.2009.151

Williams EG, Wu Y, Wolski W, Kim JY, Lan J, Hasan M, Halter C, Jha P, Ryu D, Auwerx J, et al (2018) Quantifying and localizing the mitochondrial proteome across five tissues in a mouse population. *Mol Cell Proteomics* 17: 1766–1777. doi:10.1074/mcp.RA118.000554

Xu L, Wang X, Zhou J, Qiu Y, Shang W, Liu JP, Wang L, Tong C (2020) Miga-mediated endoplasmic reticulum-mitochondria contact sites regulate neuronal homeostasis. *Elife* 9: e56584. doi:10.7554/eLife.56584

Zeileis A, Hothorn T (2015) Diagnostic checking in regression relationships. https://www.semanticscholar.org/paper/Diagnostic-Checking-in-Regression-Relationships-Zeileis-Hothorn/58b4d02ee546c30e31a3ead4ccb956fc451e6e95.

Zhang Y, Liu X, Bai J, Tian X, Zhao X, Liu W, Duan X, Shang W, Fan HY, Tong C (2016) Mitoguardin regulates mitochondrial fusion through MitoPLD and is required for neuronal homeostasis. *Mol Cell* 61: 111–124. doi:10.1016/j.molcel.2015.11.017

Zhao X, Leon IR, Bak S, Mogensen M, Wrzesinski K, Hojlund K, Jensen ON (2011) Phosphoproteome analysis of functional mitochondria isolated from resting human muscle reveals extensive phosphorylation of inner membrane protein complexes and enzymes. *Mol Cell Proteomics* 10: M110.000299. doi:10.1074/mcp.M110.000299

Zhao X, Bak S, Pedersen AJ, Jensen ON, Højlund K (2014) Insulin increases phosphorylation of mitochondrial proteins in human skeletal muscle in vivo. *J Proteome Res* 13: 2359–2369. doi:10.1021/pr401163t